Chinese Chemical Letters 37 (2026) 110665

Contents lists available at ScienceDirect

Chinese Chemical Letters

journal homepage: www.elsevier.com/locate/cclet

Anode engineering for electrocatalytic CO_2 reduction reaction

Mingming Zhang[a,1], Ting Xu[a,b,1,*], Ruonan Yin[a,1], Xueqiu Chen[a], Zheng-Jun Wang[a], Jun Li[a], Xin Wang[c], Huile Jin[a], Haibo Ke[d,*], Shun Wang[a,*], Jing-Jing Lv[a,*]

[a] Key Laboratory of Carbon Materials of Zhejiang Province, Wenzhou Key Lab of Advanced Energy Storage and Conversion, Wenzhou University, Wenzhou 325035, China
[b] College of Information Science and Electronic Engineering, Zhejiang University, Hangzhou 310027, China
[c] Department of Chemistry, City University of Hong Kong, Hong Kong 999077, China
[d] Songshan Lake Materials Laboratory, Dongguan 523808, China

ARTICLE INFO

Article history:
Received 31 May 2024
Revised 13 November 2024
Accepted 21 November 2024
Available online 24 November 2024

Keywords:
Electrocatalytic CO_2 reduction reaction
Anode engineering
Value-added oxidation reaction
Photo/bio-assistance anode
Metal-CO_2 battery

ABSTRACT

Electrocatalytic carbon dioxide reduction reaction (eCO_2RR) holds great promise in producing value-added chemicals, and achieving carbon neutrality. However, the efficiency of eCO_2RR is often hindered by the sluggish oxygen evolution reaction (OER) at the anode. Thereby, various strategies have been developed to boost anode reaction, aiming to realize economic viability and reduce energy consumption in an eCO_2RR electrolyzer. To give a comprehensive overview of anode engineering for optimizing eCO_2RR, this review summarizes and discusses the cutting-edge anodic design strategies from recent research progress. They mainly include the direct substitution of OER to the value-added oxidation reaction of other small molecules, the introduction of photo/bio-assistance anodes, and the construction of metal-CO_2 batteries. Furthermore, the emerging challenges and a forward-looking perspective on anode development by coupling renewable energy, sewage treatment and eCO_2RR are also proposed.

© 2025 Published by Elsevier B.V. on behalf of Chinese Chemical Society and Institute of Materia Medica, Chinese Academy of Medical Sciences.

1. Introduction

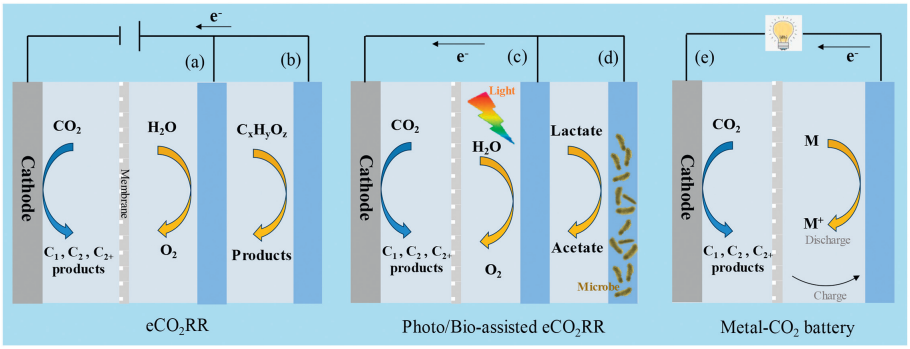
With the increasing concentration of atmospheric carbon dioxide (CO_2), serious consequences have globally prevailed, such as the climate warming, ocean acidification, and ecosystem destruction [1–4]. To address this challenge, considerable attention has been directed towards the electrocatalytic CO_2 reduction reaction (eCO_2RR) as a promising avenue for sustainable chemistry and achieving carbon neutrality [5–7]. This process holds the potential to convert CO_2 into value-added chemicals and fuels under mild reaction conditions. While massive efforts have been invested in developing cathodic electrocatalysts, microenvironments, reactor device, and related mechanism studies, aiming at boosting the efficiency of CO_2 conversion with high production and product selectivity, as well with the long-term stability [8–10]. However, bridging the gap between fundamental research and industrial application necessitates a focus on maximizing product value while minimizing the energy costs in CO_2 electrolysis [11].

In a conventional CO_2 electrolyzer, the cathodic CO_2 reduction and anodic water oxidation occur simultaneously (Scheme 1a), typically requiring an external energy input for operation [12–14]. Ongoing research and development efforts are primarily concentrated on optimizing cathodic catalysts and reaction conditions, with less emphasis on the anodic reaction and electrode [15,16]. However, the anode plays a pivotal role in eCO_2RR process, significantly determining the performance and stability of the entire electrolyzer [17–20]. Generally, the anodic process in CO_2 electrolysis involves the electrochemical water oxidation to oxygen, known as the oxygen evolution reaction (OER). As estimated, about 90 % of the total electrical input for CO_2 electrolysis is consumed at the anode for the OER [21]. This causes the critical challenges in CO_2 electrolysis, such as energy inefficiency and poor stability as resulted from the oxygen bubble disturbance [22].

Recognizing these critical challenges, recent years have witnessed a strategic shift from OER towards coupling eCO_2RR with high-efficiency anodic reactions (Schemes 1a and b), which can significantly improve energy efficiency and produce more value-added chemicals [23–25]. Moreover, innovative anodes incorporating external assistance, such as photo-anode and microbe-anodes, mark a significant breakthrough in CO_2 conversion and sustainable energy production (Schemes 1c and d) [26,27]. These advancements can alter the dilemma situation for merely relying on the

* Corresponding authors.
E-mail addresses: xuting830@163.com (T. Xu), kehaibo@sslab.org.cn (H. Ke), Shunwang@wzu.edu.cn (S. Wang), jjlyu@wzu.edu.cn (J.-J. Lv).
[1] These authors contributed equally to this work.

https://doi.org/10.1016/j.cclet.2024.110665
1001-8417/© 2025 Published by Elsevier B.V. on behalf of Chinese Chemical Society and Institute of Materia Medica, Chinese Academy of Medical Sciences.



Scheme 1. Schematic diagrams for various eCO_2RR system using (a) OER anode, (b) value-added anode, (c) photo-anode, (d) microbe-anode and (e) metal-CO_2 battery.

electricity input, accelerating the development of converting renewable resources into electricity and industrial feedstock. Furthermore, metal-CO_2 batteries have emerged as a unique and efficient approach to CO_2 utilization, offering a dual benefit of CO_2 conversion and electricity generation [13,22,28–30]. Those evolutions in anode technology underline the necessity of a comprehensive review for the research progress in anode engineering to guide the development of eCO_2RR forward to the practical market.

In this review, we delve beyond the introduction of value-added anodic reactions, to cover the most important anode breakthroughs for promoting eCO_2RR. The main research progress is structured into three sections, including the value-added anodic reactions, photo/microbe-anode in eCO_2RR, and metal-CO_2 battery anode. Each section presents some representative studies, unearths the main correlation between the anode condition and eCO_2RR activity, and points out the existing challenges along with some potential solving solutions. Finally, we offer a forward-looking perspective on the overall landscape of anode engineering for promoting eCO_2RR, outlining potential directions for future research and development.

2. Value-added anodic reactions

In general, the anode in a conventional eCO_2RR system typically involves the OER, which not only requires significant overpotential, but also brings bubble formation issues. Therefore, it is imperative to drive the anode reaction at lower operating voltages as well as generate soluble value-added products in the electrolyte. A promising strategy involves driving alternative reactions at the anode, which can substantially enhance the overall economic feasibility of the electrolyzer [31,32]. To optimize electricity usage during electrolysis, coupling eCO_2RR with anodic alternatives that demand less energy and/or yield profitable, high-value products is a promising direction. This part focuses on the latest developments in integrating eCO_2RR with concurrent alternative oxidation reactions of inorganic reactants using chloride [33,34], sulfide [35–38], ammonia [39], as well as organic reactants involving alcohols [40,41], aldehydes [23,42] and urea [43]. As summarized in Table 1 [22,44], the oxidation of inorganic and organic reactants generally shows lower overpotential and achieve more purposes at one stroke, such as sewage treatment, synthesis of new substances, and generation of electricity.

2.1. Oxidation of inorganic reactants

Chlorine ions are widely existed in the pollutant water from various industrial processes, such as disinfection, and chemical synthesis. Therefore, coupling the chlorine oxidation reaction (COR) with the eCO_2RR can be promising in sewage treatment [34]. Guo *et al.* developed a combined electrolysis system to integrate eCO_2RR with the chlor-alkali process to produces CO and Cl_2 with Faradaic efficiencies of ~98.5% and ~80% at 100 mA/cm^2, respectively [45]. Furthermore, the system yielded $KHCO_3$ at a production rate of 18 mmol/h for 5 h, achieving an energy efficiency of 39% without Ohmic drop correction (Fig. 1a). Ge *et al.* constructed a mesoporous Co_3O_4 catalyst to catalyze the anodic COR at a cell voltage of 2.7 V, driving the overall electrolysis with a voltage 1.8 V lower than that of anodic OER under the same conditions (Fig. 1b) [33]. Li *et al.* explored COR on the anode in an aqueous solution, where CO_2 could be efficiently reduced to CO while HCl was oxidized to Cl_2 [46]. Although the obtained CO and Cl_2 can be used as a feedstock to produce phosgene, the lack of a well-designed device for immediate conversion of CO and Cl_2 increases additional costs, and the corrosive nature of Cl_2 poses challenges for reactor design on a large scale.

Sulfide oxidation reaction (SOR) is another alternative anodic reaction to replace OER. H_2S is traditionally deemed as the severe harmful gas in natural gas. By integrating the eCO_2RR with H_2S oxidation reactions assisted by redox couples, CO and sulfur can be produced with high activity and stability on non-precious catalysts (Fig. 1c) [36]. Because the redox potential of EDTA-Fe^{3+}/EDTA-Fe^{2+} is 0.68 V *vs.* RHE (lower than 1.23 V *vs.* RHE), the onset potential to drive the eCO_2RR and EDTA-Fe^{2+} oxidation in a two-electrode cell was only 1.0 V, which is about 0.5 V lower than that in CO_2RR/OER system (Fig. 1d). Similarly, using an I^-/I^{3-} redox, Zhang *et al.* coupled the eCO_2RR with SOR to produce CO and S simultaneously, where the S^{2-} was oxidized by the I^{3-} to produce S in the anolyte [37]. The standard redox potential of I^{3-}/I^- (0.54 V *vs.* RHE) is lower than 0.68 V RHE of EDTA-Fe^{3+}/EDTA-Fe^{2+}. Therefore, the energy-saving efficiency of the I^{3-}/I^- redox system driving eCO_2RR/SOR is expected to outperform that of the EDTA-Fe^{3+}/EDTA-Fe^{2+} driven system.

The eCO_2RR/SOR system can significantly improve the energy efficiency of CO_2 electrolysis by replacing the traditional OER and reducing overall electrical energy consumption. It can also produce valuable chemicals such as carbon monoxide, and sulfur, which can be used as the important industrial raw materials, thereby enhancing the economic viability of the electrolysis cell and contributing to the development of a circular economy [47]. However, the corrosive substances generated during the sulfur oxidation reaction would damage the reaction equipment, and affect the stability. Future research directions may include the development of more efficient catalysts and compatible electrochemical devices to achieve more efficient eCO_2RR/SOR processes, and exploring strategies for combining with renewable energy, and waste water treatment to achieve broader industrial applications and environmental benefits.

Besides the aforementioned two eCO_2RR/COR and eCO_2RR/SOR examples, the electrooxidation of ammonia contaminants, which are abundant in agricultural runoff or industrial aqueous effluents, represents an underexplored and ideal candidate for OER replace-

Table 1
Possible oxidation of inorganic and organic reactants with the reaction equation in alkali media and the redox potentials [22,44], E^0 *versus* reversible hydrogen electrode (*vs.* RHE). The OER is also included.

	Possible anode reaction	Reaction equation in alkali media	E^0 (V)
Oxidation of inorganic reactants	$H_2O \rightarrow O_2$	$4OH^- \rightarrow O_2 + 2H_2O + 4e^-$	1.23
	$Cl^- \rightarrow Cl_2$	$2Cl^- \rightarrow Cl_2 + 2e^-$	1.36
	$S^{2-} \rightarrow S_x^{2-}$	$2HS^- + 2OH^- \rightarrow S_2^{2-} + 2H_2O + 2e^-$	0.14
	$NH_3 \rightarrow N_2 + H_2O$	$2NH_3 + 6OH^- \rightarrow N_2 + 6H_2O + 6e^-$	0.06
Oxidation of organic reactants	$CH_3OH \rightarrow HCOO^-$	$CH_3OH + 3OH^- \rightarrow HCOO^- + 3H_2O + 2e^-$	0.11
	Ethanol → Acetate	$C_2H_5OH + 3OH^- \rightarrow CH_3COO^- + 3H_2O + 2e^-$	0.06
	1,2-Propanediol → Lactic acid	$C_3H_8O_2 + 5OH^- \rightarrow C_3H_5O_3^- + 4H_2O + 2e^-$	/
	R-CHO → R-COO^- + H_2	$2R\text{-}CHO + 4OH^- \rightarrow 2R\text{-}COO^- + H_2 + 2H_2O + 2e^-$	/
	Glucose → Gluconic acid	$C_6H_{12}O_6 + 5OH^- \rightarrow C_3H_5O_3 + H_2O + 2e^-$	0.90
	Glycerol → Lactic acid	$C_3H_8O_3 + 3OH^- \rightarrow C_3H_5O_3^- + 3H_2O + 2e^-$	0.25
	Furfural → Furoic acid + H_2	$2C_5H_4O_2 + 4OH^- \rightarrow 2C_5H_3O_3^- + H_2 + 2H_2O + 2e^-$	/
	HMF → 2,5-furandicarboxylic acid	$C_6H_6O_3 + 6OH^- \rightarrow C_6H_2O_5^{2-} + 4H_2O + 4e^-$	0.3
	$CO(NH_2)_2 \rightarrow N_2 + H_2O$	$CO(NH_2)_2 + 6OH^- \rightarrow N_2 + 5H_2O + CO_2 + 6e^-$	0.07
	R-CH_2-NH_2 → R-CN	R-CH_2-NH_2 + $4OH^-$ → R-CN + $4H_2O$ + $4e^-$	/
	Octylamine → Octanenitrile	$C_8H_{19}N + 4OH^- \rightarrow C_8H_{15}N + 4H_2O + 4e^-$	/

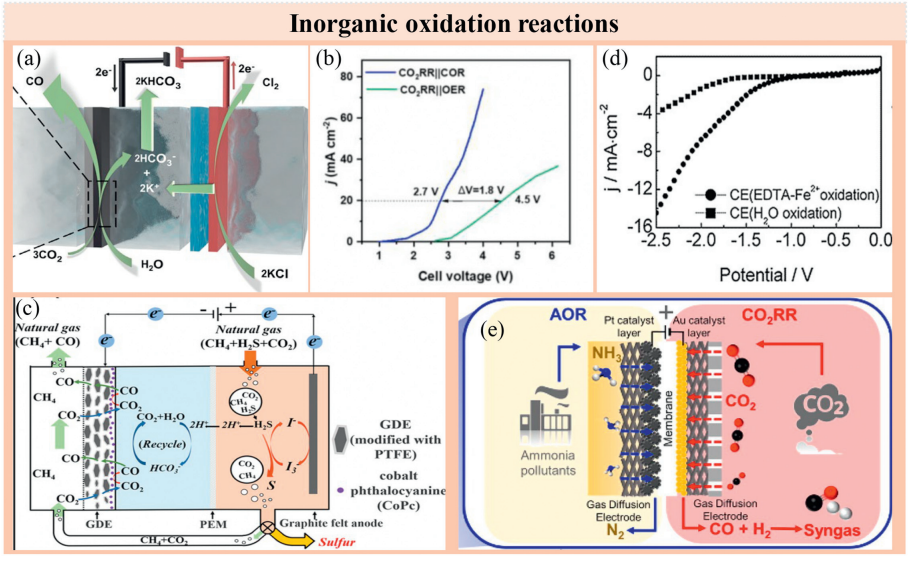


Fig. 1. (a) Schematic illustration of the paired electrolysis integrating eCO_2RR with chlorine evolution reaction. Copied with permission [45]. Copyright 2020, Elsevier. (b) LSV curves for catalysts at a scan rate of 10 mV/s in a H-type cell. Copied with permission [33]. Copyright 2022, Elsevier. (c) Operation principle diagram of the high yield of CO and synchronous efficient S recovery system. Copied with permission [36]. Copyright 2018, Wiley. (d) LSV curves of different anodic reactions on eCO_2RR in a two-electrode configuration. Copied with permission [37]. Copyright 2021, American Chemical Society. (e) Potentials and power consumption for cathodic AOR and OER. Copied with permission [39]. Copyright 2022, Elsevier.

ment [48]. Compared to using the OER, Choi *et al.* found that the thermodynamic lower overvoltage using ammonia oxidation reaction (AOR) enables a decrease in the total cell operation voltage of a maximum of 34.03 % (Fig. 1e) [39]. In a word, inorganic reactant oxidation boasts notable advantages. It necessitates a lower overpotential, minimizing energy usage and enhances electrolyzer economics by yielding valuable chemicals while cutting energy costs. Additionally, it aids sewage treatment, *e.g.*, chloride ion oxidation involving chlorine-laden wastewater, mitigating pollution and yielding useful chemicals. This kind of oxidation reaction improves electrolytic system energy efficiency, consuming less energy than OER. It also reduces oxygen bubble formation, bolstering electrolyzer stability and efficiency. Therefore, its integration with eCO_2RR promotes sustainable chemistry and carbon neutrality by converting CO_2 into practical chemicals and fuels.

2.2. Oxidation of organic reactants

Recent techno-economic analyses have suggested that substituting OER with organic oxidation reaction (OOR) is very promising to reduce full-cell voltage and increase the production of high-value products on both sides of the cell (Scheme 1b) [22,49,50]. The possible alternative anodic reactions that could be paired with eCO_2RR are summarized in Table 1, together with the redox potentials. As shown in Table 1, OORs using alcohols (methanol [40,41], ethanol [51], glycerol [21], 1,2-propanediol [52]) and aldehydes (glucose [53], furfural [54], 5-hydroxymethylfurfural (HMF) [23,42]) and amine oxidation [55] have recently received intensive attention as potential OER alternatives.

2.2.1. Alcohol oxidation

Among various alcohol species, methanol is the simplest monohydric alcohol which can be utilized to obtain formic acid for various fields such as rubber, pharmaceutical, and dye [56]. For instance, Wei *et al.* produced formic acid at both anode and cathode by the methanol oxidation reaction (MOR) and eCO_2RR, respectively (Fig. 2a) [41]. CuO nanosheets grown on copper foam were used as the anode electrocatalysts, which showed significantly high electrocatalytic activity, excellent stability, lower potential as well as high Faradaic efficiencies (FEs, maximum 91.3 % at the anode).

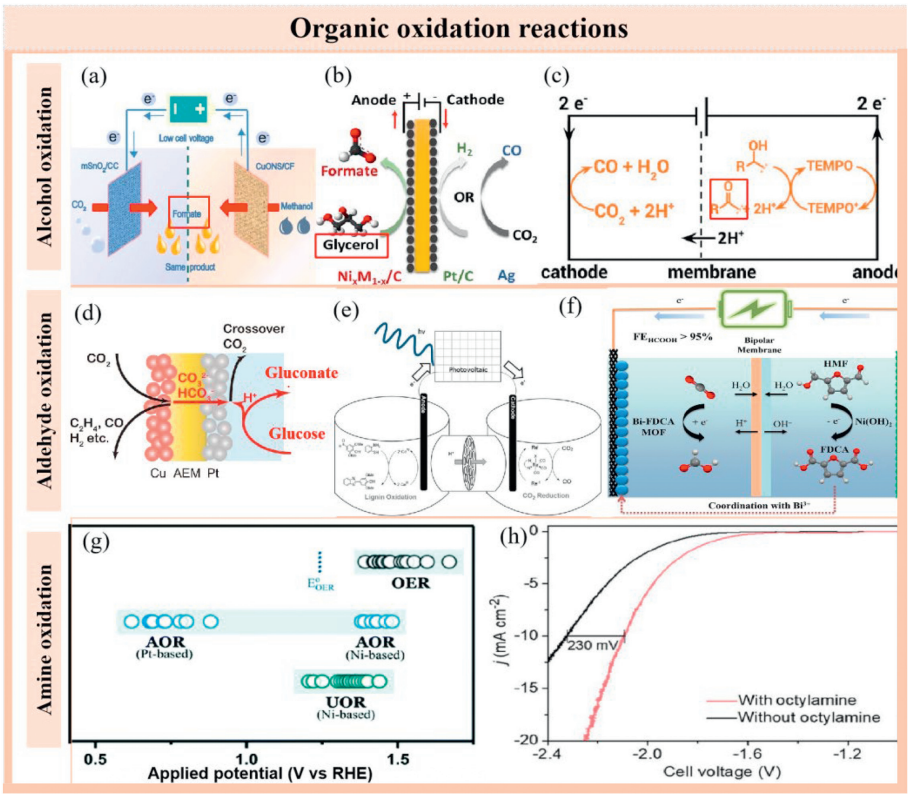


Fig. 2. Schematic illustration of an electrochemical eCO_2RR cell with (a) CH_3OH oxidation at anode. Copied ith permission [41]. Copyright 2020, Wiley. (b) Glycerol oxidation at anode. Copied with permission [58]. Copyright 2019, American Chemical Society. (c) Various alcohols oxidation at anode. Copied with permission [59]. Copyright 2018, American Chemical Society. (d) Glucose oxidation at anode. Copied with permission [53]. Copyright 2022, Elsevier. (e) Oxidation of syringaldehyde and *o*-phenyl-enediamine to give 2-(3,5-dimethoxy-4-hydroxyphenyl)-benzimidazole at anode. Copied with permission [65]. Copyright 2022, Wiley. (f) HMF oxidation at anode. Copied with permission [67]. Copyright 2022, Springer Nature. (g) Potentials for cathodic eCO_2RR-to-CO with different anodic reactions (AOR, OER, UOR) relative to RHE scale on different electrocatalysts. Copied with permission [43]. Copyright 2020, RSC. (h) LSV curves of the two-electrode electrolyzer with and without octylamine in the anodic chamber. Copied with permission [55]. Copyright 2020, Elsevier.

Similarly, Li *et al.* reported a hierarchical bifunctional CuSn alloy electrocatalyst for efficient production of nearly 100 % formate *via* simultaneous cathodic eCO_2RR and anodic MOR, which required a lower electricity input of only 2.61 $kWh/kg_{formate}$ in contrast to the 4.46 $kWh/kg_{formate}$ required for eCO_2RR coupled with OER [57].

In addition to methanol oxidation, ethanol [51] and glycerol [21] can also serve as viable options for anodic oxidation when coupled with eCO_2RR. Houache *et al.* evaluated the composition effect of carbon supported Ni_xM_{1-x} (M = Bi, Pd, and Au) nanomaterials on glycerol oxidation in alkaline media, with the anodic $Ni_{0.9}Au_{0.1}/C$ catalyst displayed the highest partial current density and the lowest onset potential when coupled with eCO_2RR (Fig. 2b) [58]. Verma *et al.* proved that coupled anodic glycerol oxidation with eCO_2RR could lower electricity consumption by up to 53 % [21]. Li *et al.* utilized the oxidation of benzylic alcohols at a platinum anode to achieve >78 % yield of acetone, while simultaneously converting CO_2 into CO at a copper-indium cathode with a current density of 3.7 mA/cm^2 and Faradaic efficiency exceeding 70 %. This alternative strategy can be extended to four different types of alcohols, producing their corresponding carbonyl compounds (Fig. 2c) [59]. Furthermore, various alcohols, such as 1,2-propanediol [52] and benzyl alcohol [60,61], have shown promise in producing more value-added products through electrooxidation. Directly combining anodic alcohol oxidation with cathodic eCO_2RR holds even more promise for expanding the product scope by withdrawing the ion exchange membrane.

During the anodic oxidation process, the different kinetics among various alcohols primarily vary their oxidation rates and the nature of their oxidation products [62]. For instance, the MOR is frequently employed as an anode reaction for coupled eCO_2RR due to its ability to generate formic acid, which aids in reducing the need for downstream product separation. MOR kinetics are relatively fast, and high Faradaic efficiency and current density could be obtained at the laboratory scale [63]. In contrast, the oxidation kinetics of other alcohols, such as ethanol and glycerol, are slower. Ethanol oxidation can yield acetic acid, while glycerol oxidation can result in glyceric acid and formic acid [52,64]. The oxidation rate and product selectivity of these reactions is highly influenced by the catalyst, electrolyte, and reaction conditions.

Furthermore, the kinetics of the anodizing reaction are also impacted by the electrolyte and membrane materials. Different ions possess varying transport capabilities within the electrolyte, and liquid products may permeate through the membrane. Consequently, selecting suitable ion exchange membranes and electrolytes is crucial for optimizing the kinetics of anodic oxidation reactions.

2.2.2. Aldehyde oxidation

Aldehydes, which can be more easily oxidized than alcohols, constitute another important class of compounds in OOR. Glucose is abundant from biomass, which can be used to produce gluconate, glucuronate, and glucarate by the electrochemical oxidation, which are feedstocks to produce biopolymers and pharmaceuticals. Xie *et al.* coupled the eCO_2RR with the glucose oxidation reaction (GOR), which showed a low full-cell voltage of 1.9 V and total carbon efficiency of 48 %, enabling 262 GJ/ton ethylene, a 46 %

reduction in energy intensity compared to conventional CO_2-to-ethylene electrolyzer (Fig. 2d) [53]. Llorente *et al*. demonstrated a paired electrolysis in the case of the oxidative condensation of syringaldehyde and *o*-phenyl-enediamine to give 2-(3,5-dimethoxy-4-hydroxyphenyl) benzimidazole coupled with the eCO_2RR to CO mediated by the molecular electrocatalysts (Fig. 2e) [65]. Integrating these two kinds of reactions in a single reactor can effectively reduce the energy demand.

Hexose, as the most abundant starting molecules from biomass, can directly be dehydrated to produce HMF and then oxidized to other valuable products, for example, its representative oxidation product, 2,5-furandicarboxylic acid (FDCA), is one of the high valuable bio-based molecules [25,42,66]. Choi *et al*. successfully demonstrated eCO_2RR could be coupled with the anodic oxidation of HMF under near-neutral conditions by synthesizing 5 nm nickel oxide nanoparticles, exhibiting an anodic current onset (1 mA/cm^2) at 1.524 V *vs.* RHE and a total Faradaic efficiency of ~70% (Fig. 2f) [67]. Moreover, FDCA is also a class of biobarboxylic acid ligands that can coordinate with metal ions to demonstrated high selectivity in catalyzing the eCO_2RR to formic acid at a potential of -1.2 V *vs.* RHE and a total current density of 19.6 mA/cm^2, achieving a FE of over 95%. By assembling the two half-reactions in a single electrolytic cell, they were able to simultaneously obtain formic acid with a FE of 95.6% and FDCA product with a FE of 75.0%. This work provides an economic and environmental strategy for the more efficient utilization of anode and cathode products.

2.2.3. Amine oxidation

In addition to the alcohol and aldehydes reactants, other organic substrates like primary amines also have low oxidation potentials. Medvedeva *et al*. investigated the coupling of eCO_2RR with ammonia and urea oxidation reactions (AOR and UOR). They compared the reported anodic onset potentials for AOR, UOR and OER on Pt-based or Ni-based catalyst (Fig. 2g) [43]. Although AOR has a very low standard potential, it suffers from electrode deactivation due to the formation of absorbed nitrogen intermediates (N_{ads}) and be efficiently used in a CO_2-electrolyzer. Further studies can focus on the development of efficient and low-cost SOR-, AOR- or UOR-catalysts capable of handling N_{ads}, improving eCO_2RR performance and energy efficiency of the overall cell, and providing additional economic and environmental benefits for the practical application. By introducing the oxidation process of octylamine using Ni_2P as the anode material (Fig. 2h), the operating cell voltage of the co-electrolysis process is reduced by 230 mV compared to the traditional OER [55]. Like the previously reported HMF oxidation process [25,42], the operating voltage of the electrolytic system is 2.2 V at an operating current density of approximately 20 mA/cm^2. This phenomenon can be attributed to the slow kinetics of the eCO_2RR at the cathode and the mass transfer limitations of the anode reactants [55]. However, the stability of electrolysis is not studied in this study, which affects the possibility of its practical application.

These OORs electrochemical studies highlight the opportunity to create an electrolyzer generating higher value-added chemicals at both electrodes, making them superior substitutes for OER. However, although it is relatively easier to achieve high selectivity for MOR to formic acid product (approaching 100%) at the anode, it is still tough to achieve a single C_{2+} organic products with benchmark selectivity over 70%. In addition, significant research into the development of bifunctional electrocatalysts and compatible electrochemical devices for the co-electrolysis of anodic and cathodic reactions would be needed to make the process close to practical market.

In conclusion, this section summarizes the coupling eCO_2RR with the oxidation of inorganic and organic reactants. The oxidation of organic reactants enables the generation of valuable chemicals with high selectivity and a reduction in the overall battery voltage. Especially, the oxidation of chlorine ions can be promising in sewage treatment and integrated with the chlor-alkali process to produce CO and Cl_2 with high Faradaic efficiencies. SOR is another alternative anodic reaction that can replace OER, producing CO and sulfur with high activity and stability on non-precious catalysts. However, it also presents challenges related to corrosive properties and the management of by-products. The oxidation of organic reactants, such as methanol, ethanol, and glucose, enables the generation of valuable chemicals with high selectivity and a reduction in the overall battery voltage. Meanwhile, challenges persist in terms of product selectivity and equipment design. Value-added anodic reactions of other small molecules have the potential to enhance the efficiency and economic viability of the eCO_2RR, while simultaneously increasing environmental benefits. For instance, integrating wastewater treatment with eCO_2RR can reduce energy consumption and add value to the overall process. Future research will need to focus on improving reaction selectivity, developing compatible electrochemical devices, and optimizing reactor design.

3. Photo/bio-anode in eCO_2RR

Motivated by the goal to reduce or even eliminate the reliance on the external electrical energy, the anode has been upgraded to converse other renewable energy resources into electricity within the eCO_2RR system. These upgraded anodes mainly include two categories: Photo-anode and bio-anode [27]. The former is to transform the solar energy into electrical energy, while the latter can capture the chemical waste to generate electricity.

3.1. Photo-anode-assisted eCO_2RR system

Photoelectrochemical (PEC) CO_2RR using semiconductor photoelectrodes with solar illumination has attracted great attention (Scheme 1c) [68,69]. It integrates the advantages of both electrocatalytic and photocatalytic conversion methods, which can not only reduce the atmospheric CO_2 concentration economically, but also convert CO_2 into valuable fuels and chemicals with environmental benefits [70]. One of the key challenges in photocatalysis is to design a catalyst that can absorb light and produce electron-hole pairs efficiently with suitable redox potential. Thus, the following section will focus on the catalysts and the anodic enhancement strategies in the developed photocatalysis systems.

3.1.1. Titanium dioxide (TiO_2)-based catalysts

Currently, TiO_2 is the one of the most extensively studied photocatalysts because of its low cost, long hole diffusion length, photo-stability and environmentally friendly characteristics [71,72]. Nevertheless, TiO_2 presents two major limitations: (1) High recombination of electron-hole pairs and (2) low purity and crystallinity [73,74]. A promising way to depress the recombination of electron–hole pairs is to associate TiO_2 with metal co-catalyst. Meanwhile, improving the purity and crystallinity of TiO_2 is mainly achieved by doping and improving the synthesis method [75]. In this respect, morphology variation, metal particle decoration and composite formation of TiO_2 have been recently investigated to improve electron mobility, chemical stability, and hence the photoconversion efficiency.

Bare TiO_2: Commercial TiO_2-P25 has been the most investigated light-responsive material in PEC CO_2RR systems [76]. Castro *et al*. coupled TiO_2-P25 nanoparticle photoanode and Cu plate cathode for the continuous conversion of CO_2 to alcohols. A maximum increment of 4.3 mA/cm^2 in current density between the UV illumination ($j = 9.9$ mA/cm^2) and the dark experiment ($j = 5.6$ mA/cm^2) conditions was achieved at -2 V *vs.* Ag/AgCl [75]. TiO_2 nanoparticles with enhanced optical properties, large surface area, appro-

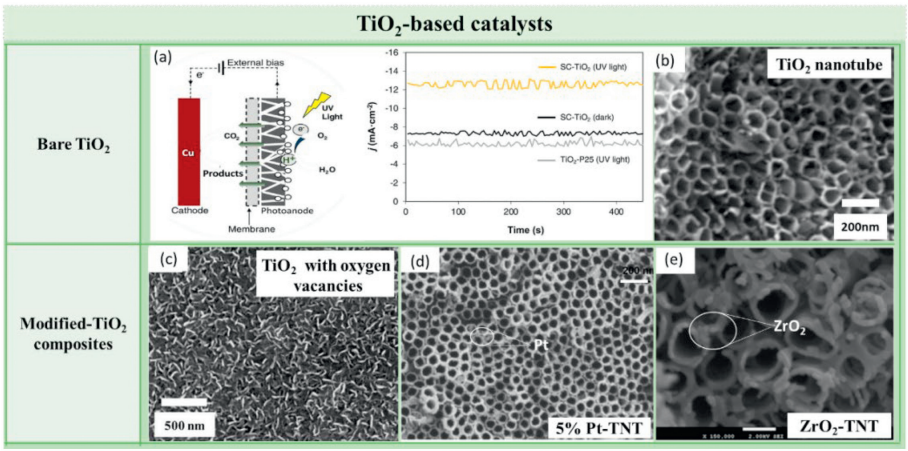


Fig. 3. (a) Schematic illustration of the photoanode (MEA)/dark cathode configuration and current density evolution at -1.8 V *vs.* Ag/AgCl for SC-TiO_2 photoanodes. Copied with permission [71]. Copyright 2022, Elsevier. SEM images of (b) TiO_2 nanotube, Copied with permission [77]. Copyright 2020, American Chemical Society. (c) 2D leaf-like TiO_2 nanosheets with oxygen vacancies. Copied with permission [78]. Copyright 2021, Elsevier. (d) 5 % Pt-modified TiO_2 nanotube. Copied with permission [81]. Copyright 2016, American Chemical Society. (e) ZrO_2-modified TiO_2 nanotube. Copied with permission [82]. Copyright 2019, Elsevier.

priate morphology, and superior crystallinity synthesized in supercritical medium (SC-TiO_2, $j = 12.31$ mA/cm^2) by Ivan *et al.* were markedly superior to the commercial TiO_2-P25 ($j = 5.9$ mA/cm^2) photoanodes under the same reactor configuration and experimental conditions (Fig. 3a) [71]. The SC-TiO_2 photoanode could drive CO_2 conversion to produce more products, which could be mainly ascribed to the superior photocurrent densities that affected the selectivity of the reaction. However, further efforts are still required to improve the photocatalytic performance, especially for the photoconversion efficiency. TiO_2 nanotubes present higher catalytic activity and larger specific area, in comparison with other TiO_2 nanostructures. Zhang *et al.* designed a CO_2 self-driving and self-recycling photocatalytic cell which CO_2 produced from wastewater degradation in the anode can be converted to C_1 fuel at the cathode [77]. The TiO_2 nanotube photoanode oxidized organic pollutant to CO_2, which achieved an increase of 40 % in organics removal and an extra C_1 fuel yield rate of 6.7 μmol g^{-1} h^{-1}, compared to the conventional photocatalytic system (Fig. 3b).

Enhancing its photocatalytic performance, the purity and crystallinity of TiO_2 are crucial to its efficacy as a photoanode. High purity TiO_2 can minimize electron-hole pair recombination, thereby enhancing the transfer efficiency of photogenerated electrons, while good crystallinity ensures efficient electron transport within the semiconductor [75]. Wang *et al.* used sequential hydrothermal and calcination processes to obtain TiO_2 particles. The chloride was used during the hydrothermal process to enhance the formation of oxygen vacancies and defects on the TiO_2 surface, which endowed the TiO_2 photoanode with superior PEC capacity (Fig. 3c). Moreover, the calcination treatment improved the crystallinity and anatase/rutile ratio to further enhance its PEC capacity [78]. An optimized sol-gel method for TiO_2 coating was developed for CO_2 photoreduction [79]. Polyethylene glycol was used to slow down the growth of crystals as it has a high affinity for water, which slowed down the initial evaporation rate of water. Consequently, this facilitated the achievement of TiO_2 particles with superior crystallinity. However, TiO_2 has a high band gap between 3.2 eV and 3.4 eV, making it sensitive to UV light, which composes less than 5 % of the solar spectrum. Researchers have come up with various methods to improve its photocatalytic activity and solar energy utilization rate.

Modified-TiO_2 composites: The modification on TiO_2 has also been applied into the design of photoanodes. Peng *et al.* reported a nitrogen-doped TiO_2 thin film (NTTF), in which the pure TiO_2 target prepared from P25 Degussa particles was ablated with a pulsed laser under nitrogen and oxygen atmosphere, as the photoanode in the PEC system [80]. The NTTF has a band gap of 2.0 eV and can be excited by the visible light. Except for doping metal-free elements, decorating noble metal species has been applied to TiO_2. Noble metals with low Fermi level are expected to trap electrons and inhibit the recombination of photogenerated electron-hole pairs. Zhang *et al.* electrodeposited Pt on to TiO_2 nanotube under a constant current of 2 mA/cm^2 to obtain a Pt-modified TiO_2 nanotube (Pt-TNT) photoanode [81]. Pt nanoparticles were subjected to galvanostatic deposition on the TNT anode to inhibit the recombination of photogenerated electron−hole pairs and improve its photocatalytic activity. Pt-TNT anode with a Pt loading amount of 5 % could achieve high carbon atom conversion rate of 1250 nmol h^{-1} cm^{-2} (Fig. 3d). By coupling other semiconductors to form a new structure can also improve optical properties of TiO_2. The conduction band of ZrO_2 could be slightly lower than that of TiO_2 due to the present of defects, which could amplify the performance of the photoanode in relation to the bare TiO_2 nanotube. Brito *et al.* modified TiO_2 with ZrO_2 by a wet-chemical deposition method, which the TiO_2 was immersed in $ZrCl_4$ solution, driving the electrons to the cathode side saturated with CO_2 promoted generation of around 3.8 mmol/L of methanol and 0.96 mmol/L of ethanol under TiO_2 nanotube-ZrO_2 photoanode (Fig. 3e) [82]. Similarly, Riza *et al.* electrodeposited Cu_2O on TiO_2 nanotube arrays by a square wave voltammetry electrochemical deposition method to form heterojunctions and enhanced photogenerated charge separation, which has been demonstrated with better photocatalytic activity than that of TNA/Ti due to the UV–visible light absorption of Cu_2O [83].

3.1.2. Other metal catalysts

Photo-corrosion phenomenon widely exists on photoanode which results in decreased stability. It has been demonstrated that the stability and catalytic performance of photoelectrode can be improved by the surface modification [84,85]. GaN-based materials have garnered attention for CO_2 reduction because of their excellent optical properties and band structure. Chen *et al.* studied the photocatalytic performance of different In contents in $In_xGa_{1-x}N$ photoanodes and found that the photoanode containing 0.9 % In enhanced the CO_2 conversion. However, severe photo-corrosion of GaN-based photoelectrode greatly limits their applications [86]. Meanwhile, as a traditional two-dimensional photocatalyst, carbon nitride (C_3N_4) is thermally and chemically stable but with a poor catalytic ability due to the restacking of two-dimensional

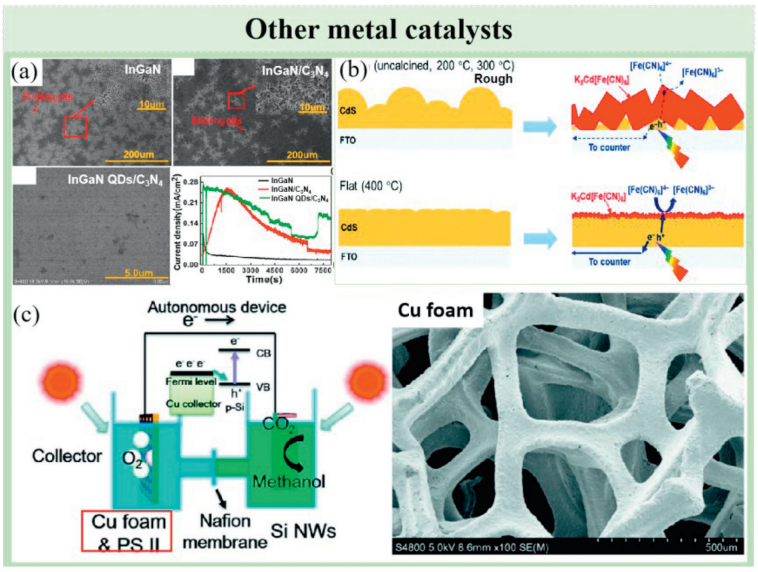


Fig. 4. (a) Schematic illustration of the InGaN quantum dots (QDs) combined with C_3N_4 nanosheets photoanode. Copied with permission [87]. Copyright 2019, Elsevier. (b) Schematic illustration of the CdS photoanode calcined at 400 °C. Copied with permission [88]. Copyright 2019, Elsevier. (c) Schematic illustration and SEM image of the Cu foam photoanode combined with PS-II. Copied with permission [89]. Copyright 2019, Elsevier.

layered materials in the catalytic reaction process [68]. Based on these characteristics, Xing *et al.* improved the photocatalytic activity and stability by combining InGaN quantum dots (QDs) with C_3N_4 nanosheets as photoanode. As convinced in Fig. 4a, the photoelectron-chemical corrosion of InGaN QDs/C_3N_4 has been apparently suppressed. QDs and C_3N_4 can accelerate the separation of photogenerated electron–hole pairs and avoid the accumulation of holes, and then inhibit photoelectrochemical corrosion [87].

Metal sulfides are also promising visible-light photocatalysts for CO_2 reduction. However, available sulfide photocatalysts are limited because of their instability in aqueous solutions under photoirradiation. For instance, pure CdS is easy to be corroded by light, resulting in unstable photoelectric performance. Masanobu Higashi *et al.* fabricated a stable CdS photoanode for CO_2 reduction and the CdS electrode calcined at 400 °C had a smoother surface, with a lower surface area of the electrode, which consequently reduced the CdS photocorrosion [88]. A high concentration of photogenerated holes caused photo-corrosion of CdS, thus reducing the photocurrent. The addition of $K_4[Fe(CN)_6]\cdot 3H_2O$ to borate buffer solution can effectively scavenge photogenerated holes in CdS and enable the oxidation of $[Fe(CN)_6]^{4-}$ to $[Fe(CN)_6]^{3-}$ (Fig. 4b). Moreover, reducing the contact between light and photoanode would be helpful to alleviate the photo-corrosion. Lian *et al.* chose an efficient light-driven water oxidizing enzyme, photo-system II (PS-II), which could accelerate the capture of a relatively wide range in the sunlight spectrum [89]. In the PS-II process, photo-induced electrons were transferred through several intermediate processes to finally reach the Q_B site (electron acceptor) in the chlorophyll matrix, and then, electrons from Q_B could quickly transfer to Cu foam to allow the following reaction to occur (Fig. 4c).

Indeed, there is still room to increase the current density, as all these photoanode-assisted PEC CO_2RR were carried out in H-type cell. The flow cell is a promising way to improve the energy utilization efficiency, in which the photoanode needs to generate a significant high photocurrent. Silicon (Si) emerges as a promising photoanode candidate in driving the PEC CO_2RR in flow cell due to its high saturation current density (larger than 40 mA/cm^2) [90,91]. Now, researchers utilized the back-illuminated nonmetallic Si photoanode to assist PEC flow cell which showed a solar-to-fuel (STF) efficiency [69]. In the future, more advanced metal-free and high STF conversion materials should be introduced as photoanodes in the flow cell or other large-scale reactors.

3.2. Bio-anode-assisted eCO_2RR systems

Bioanode-assisted system represents a promising new avenue for eCO_2RR, leveraging the chemical energy of waste to convert it into electrical energy through the decomposition of organic matter such as waste water, food waste, by microorganisms [28,92]. These microorganisms can grow on anode surfaces, acting as biocatalysts to oxidize organic matter and transfer electrons to the cathode [93–95]. Based on the different properties, bioanodes can be categorized into two types: (1) Enzyme-involved anode and (2) microbe-involved anode [96,97]. However, limited reports on combining enzyme-involved anodes with eCO_2RR systems, possibly due to the higher cost and lower stability relative to microbe-involved anode.

Currently, in a typical microbial electrochemical (MEC) system, the waste organics are degraded by the electroactive microorganisms in the anode chamber, which can donate more electrons to the cathode to increase system current and reduce potential compared with OER, thereby increasing the rate of cathode eCO_2RR and improving the generation of cathode products [27,98–100]. Zhao *et al.* applied a pair of iron–graphite electrode to improve sludge anaerobic digestion of acetate and reduce CO_2 into formate with a production rate of 672.3 mg/L under a low applied potential of −0.6 V (Fig. 5a) [101]. However, the acetate concentration in all the reactors first decreased and then rapidly increased before the seventh day. Therefore, the stability of the catalyst needs further improvement. Tian *et al.* developed a microbial reverse-electrodialysis cell to reduce CO_2 on Bi/Cu electrode by extracting sustainable energy from wastewater and salinity gradient at the graphite fiber brush anode (Fig. 5b) [95]. The stability of output current and cathode potential was adjusted by the chemical oxygen demand (COD) load. An optimal anodic COD load of 1 g/L NaAc provided more available substrate for microorganisms to convey more electron production through the external circuit, thereby promoting the formate production and enhancing system stability. Further study should focus on how to get higher and more stable product production by changing fed batch mode or more robust catalysts. Similarly, Luo *et al.* reported similar studies in which they

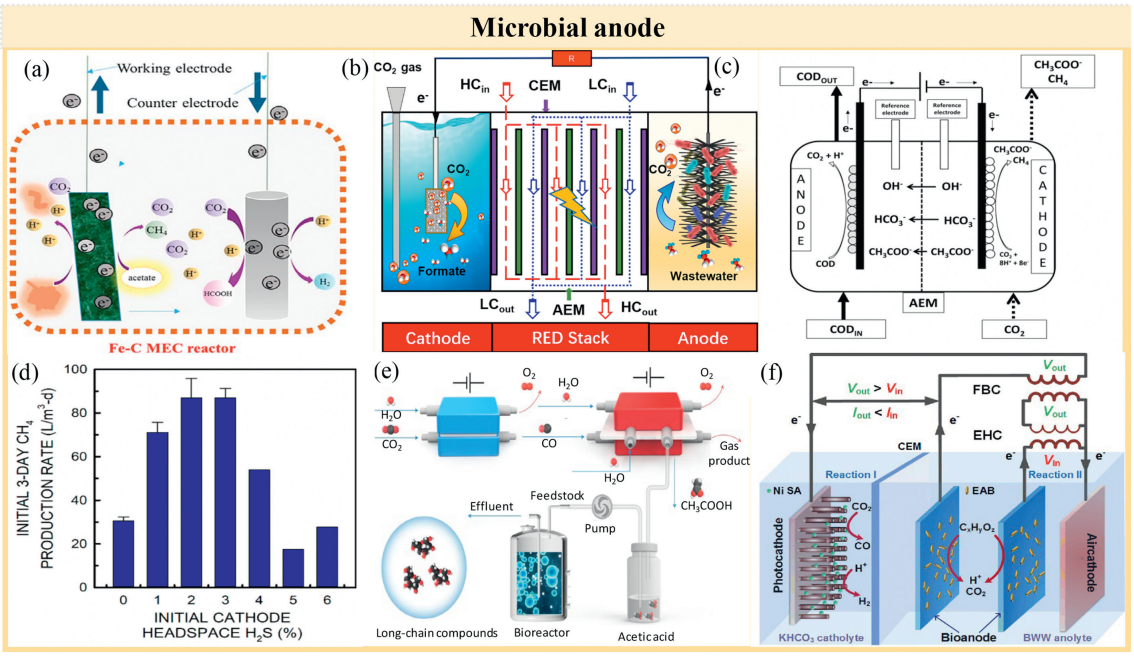


Fig. 5. (a) Schematic illustration of microbial electrosynthesis system. Copied with permission [101]. Copyright 2016, Elsevier. (b) Schematic illustration of the microbial reverse eCO_2RR cell as well as assembly diagram of the membrane stack. Copied with permission [95]. Copyright 2021, Elsevier. (c) Schematic illustration of the microbial electrolysis cell under continuous flow mode operation. Copied with permission [103]. Copyright 2021, Wiley. (d) Initial 3-day mean methane production rate by the sulfide-amended bioelectrochemical system at initial cathode headspace H_2S concentration (v/v) of 0–6%. Copied with permission [104]. Copyright 2021, Elsevier. (e) Schematic illustration of the *in vitro* artificial sugar synthesis system. Copied with permission [105]. Copyright 20,222, Elsevier. (f) Schematic illustration of the photocathode and bioanode electrolysis cell. Copied with permission [93]. Copyright 2020, Elsevier.

used a 3D-structured RGO-Ni catalyst as a cathode to reduce CO_2 to ethanol with a production rate of 27.8 mg L^{-1} h^{-1} and an activated carbon adhesion source for Shewanella as an anode [100].

The above anodic anaerobic digestion of organic wastes typically produces methane-rich biogas, considerable amounts of 30%-40% CO_2 and little hydrogen sulfide (H_2S), which hinders efficient utilization of biogas. To date, extensive research has focused on the biogas purification and upgrading technologies utilizing the MEC system [102]. Cristiani *et al.* reported an innovative fully biological MEC system, in which a closed-loop electron cycle between the anode and cathode allows the synthetic biogas for CO_2 removal to be flushed in the cathodic chamber (Fig. 5c) [103]. The closed-loop circuit could be an attractive way to accomplish biogas upgrading. However, the H_2S content in the biogas needs to be removed as well. Dykstra *et al.* utilized methanogenic bioelectrochemical systems to remove and utilize biogas H_2S, biocathodic CH_4 production increased by two-fold to 3.55 ± 0.17 mmol/L as the H_2S increased from 0 to 2 vol% through electron donation to the anode, which is promising for the future development of biogas upgrading and eCO_2RR technology (Fig. 5d) [104].

However, microbial attachment suffers from several drawbacks. It is only viable for a limited subset of organisms, mostly anaerobic microbes that follow the reductive acetyl-coenzyme A (acetyl-CoA) pathway, resulting in a limited product scope, primarily acetate and methane [105,106]. Another major concern is that such designs operate at very low current density, in the range of 1–10 mA/cm^2, while electrochemical production of electron carriers such as formate and acetate can operate at hundreds of milliamperes per square centimeter. The low current density is essential for the tolerance of microbial-cathode attachment systems. Furthermore, a simple calculation by Bar-Even *et al.* [105] shows that these constraints in microbial electrosynthesis would be almost impossible to overcome due to the disparities between the electrochemical system and the biochemical system, highlighting the potential value of spatially decoupling the two processes. Schmid *et al.* have demonstrated the possibility of converting CO_2 into a butanol/hexanol mixture by coupling a CO_2 electrolyser with a fermentation module in a spatially separate manner, where the syngas from the CO_2 electrolyser was used as the feedstock [106]. However, the low solubility of the gaseous feed limits the productivity of the system. A three-step pathway is projected by Zheng *et al.* for synthesizing a long-chain compound from CO_2 based on the spatially decoupled electro-biosystem (Fig. 5e). CO_2 was initially transformed into pure acetic acid *via* a two-step electrolysis process; subsequently, this intermediate was directly utilized for microbial fermentation within a bioreactor, leading to the production of long-chain compounds, such as glucose [105].

Microbial electrochemical systems have great potential in capturing chemical waste to generate electricity [92], but their performance and application potential are limited by the selection of microorganisms, system stability, and long-term operational capabilities. Selecting the appropriate microorganisms is crucial, as different microorganisms have different electron transfer efficiencies and metabolic capabilities for specific substrates. For example, some microorganisms can effectively reduce CO_2 to formic acid, acetic acid, or other valuable chemicals, while others may be more suitable for generating electricity. Therefore, selecting microorganisms that efficiently convert target substrates can significantly improve the system's performance and product selectivity. System design needs to consider the growth conditions of microorganisms, such as pH, temperature, and substrate supply, to ensure long-term stable operation. In addition, the biocompatibility and corrosion resistance of electrode materials are crucial for maintaining microbial activity and electrode performance. Future research needs to focus on these aspects to improve the overall efficiency and reliability of the system.

Moreover, integrating photocathode and bioanode technologies with eCO_2RR harnesses the strengths of both solar energy conversion and biological catalysis, offering a promising approach for sustainable and efficient CO_2 utilization. Lu *et al.* employed sili-

Table 2
Electrochemical properties of anode materials and discharge products.

Materials	Possible anode reaction	Standard reduction potential (V)	Theoretical specific capacity (mAh/g)	Typical discharge product	Gibbs free energy of formation (kJ/mol)	Standard reaction potential (V)
Li	$Li^+ + e^- \rightarrow Li$	−3.04	3860	$2Li_2CO_3 + C$	−1132.12	2.8
Zn	$Zn(OH)_4^{2-} + 2e^- \rightarrow Zn + 4OH^-$	−1.285	820	$Zn(OH)_4^{2-} + CO$	−553.5	1.2
Na	$Na^+ + e^- \rightarrow Na$	−2.713	1165	$2Na_2CO_3 + C$	−1044.4	2.35
Al	$Al^{3+} + 3e^- \rightarrow Al$	−1.676	2980	$2Al_2(CO_3)_3 + 3C$	/	/
Mg	$Mg^{2+} + 2e^- \rightarrow Mg$	−2.356	2205	$Mg(HCO_3)_2$	/	/
K	$K^+ + e^- \rightarrow K$	−2.924	685.5	$K_2CO_3 + CO$	−1063.5	2.48

con nanowires loaded with single-atom Ni catalysts as the photocathode, carbon brushes with electrically active bacteria as the bioanode, and utilized organic wastewater from a brewery as the feedstock [93]. Compared to abiotic water oxidation using PEC anodes, microbial anodes are capable of oxidizing waste organics in wastewater while reducing the oxidation potential from 1.34 V to 0.24 V, corresponding to 80 % in energy saving (Fig. 5f). Overall, these studies demonstrate a promising avenue for enhancing the efficiency of CO_2 conversion through the photo/bio-assisted eCO_2RR system. The integration of photocathode and bioanode technology appears to be able to bring superior energy saving, positively degrading environmental pollutants and converting biomass derivatives to value-added chemicals but is still at a relatively infancy stage. Moreover, as these anode materials inherently suffer from poor bacterial attachment, the ongoing research may focus on this theme and, more effectively, further improve the eletrolyzer stability.

4. Metal-CO_2 battery anode

Metal-CO_2 batteries represent an economical and efficient CO_2 utilization technique, which provides a mechanism combining CO_2 reduction with electricity generation instead of electricity input (Scheme 1e) [107–109]. Moreover, metal-CO_2 battery technology has the potential to provide a cost-effective energy storage system for renewable energy networks with greater safety and higher energy density than lithium-ion batteries [110].

Generally, metal-CO_2 batteries contain a metal anode (Li, Zn, Mg, K, Na, Al, *etc.*), an electrolyte (aqueous, nonaqueous or solid), an ion-conducting separator and a cathode to drive CO_2 conversion, respectively [29,30]. During the discharging mode, the metal anode is oxidized to give out electrons, which pass through the external circuit to reach the cathode using the incoming electrons to capture and reduce CO_2 [111,112]. The following is the discussion of anode materials, electrolytes and anode interfacial interaction for improving metal-CO_2 battery performance and stability by investigating anode behavior.

4.1. Anode materials

The anode materials significantly impact the electrochemical performance of the metal–CO_2 battery on two aspects: (1) The physical and chemical properties of the anode materials place an upper theoretical limit on the operating voltage and practical capacity; (2) The choice of anode material can change the discharge and charge process significantly. Over the past, the anode of metal-CO_2 batteries has achieved significant breakthroughs [107]. To gain insight into the variations among distinct anode materials, Table 2 offers a concise overview of their electrochemical attributes [108,109,113]. These encompass fundamental parameters like the half-reaction, standard reduction potential, theoretical specific capacity, and experimental properties, such as the prevalent discharge product, its formation energy, and the standard reaction potential.

As can be concluded from the Table 2, Li–CO_2 batteries outperform the other ones due to their impressive theoretical energy density of 1876 Wh/kg [114]. Although Na and K, as alternative alkali metal anodes, they are less energy-dense compared to lithium, they show lower formation energy for products and offer cost benefits [107]. In contrast, metals such as magnesium, aluminum, and zinc engage in multiple electron transfer processes, enabling them to attain higher theoretical capacities disproportionate to their weight. These anodes exhibit reduced reactivity compared to alkali metals and possess lower voltage windows, potentially widening the applicability of various electrolytes and cathodes. The subsequent section delves into the unique characteristics of each metal type employed as anodes in metal-CO_2 batteries.

4.1.1. Alkali metals (Li, Na and K)

The anode for an alkali metal cell is typically alkali metal foil, and the cathode is usually nanostructured carbon. Li–CO_2 is considered as a potential candidate due to high operating voltages and large theoretical specific energy density, which can provide sustainable power for long-distance transportation, especially at a high CO_2 content [29]. Liu *et al.* first designed rechargeable Li-CO_2 battery operated by using gold mesh cathodes at room temperature, detecting the reversible formation and decomposition of amorphous carbon and Li_2CO_3 ($4Li + 3CO_2 \rightarrow 2Li_2CO_3 + C$) [115]. However, the accumulation of Li_2CO_3 will increase the internal resistance of the system, resulting in the low energy efficiency and poor cycle performance [116,117]. Therefore, it is essential to develop robust and efficient catalysts capable of enhancing the decomposition kinetics of Li_2CO_3 to Li^+ for the charging process. It is found that the introduction of Ru catalyst with special electronic structure gives excellent decomposition ability of Li_2CO_3. Zou *et al.* found that a strong interaction between small Ru and Li_2CO_3, which can destabilize Li_2CO_3 and facilitate its decomposition due to the reduced binding energy of C=O and Li–O (Fig. 6a) [118]. Although the reversible reactions at low voltages can be achieved with the help of catalysts, the specific catalytic mechanism needs further exploration.

In 2016, Hu *et al.* pioneered the design of rechargeable Na–CO_2 battery based on $NaClO_4$/TEGDME electrolyte and Ni mesh coated by TEGDME-treated multiwall carbon nanotube (MWCNT) cathode (Fig. 6b) [119]. These batteries demonstrated high reversible capacity and stable cycling performance. The exceptional performance was closely associated with the battery's operational reversibility. However, the thermodynamic stability of Na_2CO_3 is comparable to that of Li_2CO_3, necessitating a higher charging voltage for its decomposition, which severely hampers the development of Na–CO_2 batteries. Consequently, researchers have investigated various catalysts to enhance the reversibility and cycling performance of these batteries. The reversible reaction of Na_2CO_3 has been discovered through several electrochemical methods, including X-ray diffraction (XRD) and X-ray photoelectron spectroscopy (XPS). Furthermore, the reversibility of carbon and CO_2 has also been confirmed. Building on this research, the superior reversible electrochemical mechanism of Na–CO_2 batteries was first proposed ($4Na + 3CO_2$

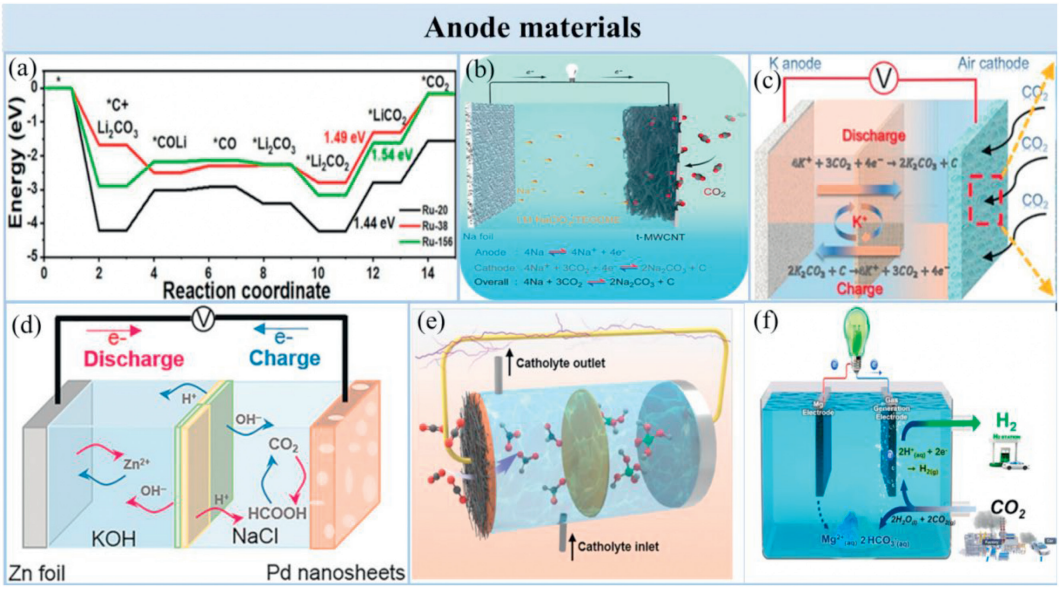


Fig. 6. (a) Gibbs free energy diagram of Li–CO_2 battery during charge. Copied with permission [118]. Copyright 2024, ACS. (b) Schematic illustration of Na–CO_2 battery. Copied with permission [119]. Copyright 2016, Wiley. (c) Schematic illustration of K–CO_2 battery. Copied with permission [120]. Copyright 2020, Wiley. (d) Schematic illustration of Zn–CO_2 battery. Copied with permission [123]. Copyright 2018, Wiley. (e) Schematic illustration of Al–CO_2 battery. Copied with permission [125]. Copyright 2023, Wiley. (f) Schematic illustration of Mg–CO_2 battery. Copied with permission [126]. Copyright 2021, Elsevier.

$\rightarrow 2Na_2CO_3 + C$). This study further provided a foundation for the application of metal-CO_2 batteries in electrochemical energy storage systems.

The plentiful and low-cost potassium in the Earth's crust has spurred the advancement of K–CO_2 batteries. In 2019, Zhang and colleagues introduced K-CO_2 batteries using carbon-based, metal-free catalysts [120]. They proposed that during discharge, K^+ ions migrate from the anode to the cathode, where they react with dissolved CO_2 to form K_2CO_3 and carbon on the cathodic carbon catalyst (Fig. 6c, $2K + 2CO_2 \rightarrow K_2CO_3 + CO$). During charging, K_2CO_3 is converted back into K^+ and CO_2 through the oxidation of carbon facilitated by the metal-free carbon catalyst. They also integrated DFT calculations with experimental findings to elucidate the reaction mechanism, which includes the reversible formation and decomposition of K_2CO_3. However, the authors only demonstrated the reversibility of K_2CO_3, and the experimental evidence was insufficient to confirm the reversible formation and decomposition of carbon. Therefore, the internal reaction mechanism of K–CO_2 batteries remains a challenging puzzle to solve.

Despite the promising potential demonstrated by alkali metal-based CO_2 batteries, their highly reactive nature significantly impedes their performance. Consequently, these batteries are predominantly operated within nonaqueous systems, which restricts the diversity and quantity of carbonaceous products. This, subsequently, presents formidable challenges for the practical deployment and widespread utilization of alkali metal-CO_2 batteries in industrial scenarios.

4.1.2. Non–alkali metals (Zn, AL and Mg)

The activities of Zn and Al are lower than that of alkali metals, which reduce the need for anhydrous and oxygen-free environments in Zn–CO_2 and Al–CO_2 electrochemical systems [121,122]. Following lithium, Zn–CO_2 batteries have received the most attention. To enhance the solubility of zinc ions, the anodic electrolyte is typically alkaline. Wang *et al.* proposed and realized an aqueous reversible Zn–CO_2 battery conducted in 1 mol/L KOH anolyte (Fig. 6d) [123]. During discharge, the zinc anode dissolves and releases electrons, and CO_2 accepts electrons and is reduced to formic acid (HCOOH); during charging, metallic zinc is deposited on the anode, while formic acid loses electrons and is oxidized back to CO_2 ($Zn + CO_2 + 2H^+ + 2OH^- \leftrightarrow ZnO + HCOOH + H_2O$). The Zn–$CO_2$ battery can be recycled for 100 times with an energy efficiency of up to 81.2 %. Notably, these reversible aqueous Zn–CO_2 batteries offer a long-term chemical production process during discharge and a highly efficient energy storage process during charge.

Aluminum, with its three-electron reaction, low molecular weight, and high abundance, is an excellent candidate for the anode in metal–CO_2 batteries [124]. Li *et al.* constructed aqueous Al–CO_2 batteries with $Cs_3Bi_2I_9$ cathode an Al anode in 1 mol/L KOH electrolyte (Fig. 6e) [125]. The Al–CO_2 battery discharges at 0.3 V for 1 h, maintaining a relatively stable current density of 22 mA/cm^2, and achieves an average formate Faradaic efficiency of approximately 89.6 %. The chemical reaction mechanism responsible for this performance is $4Al + 9CO_2 \leftrightarrow 2Al_2(CO_3)_3 + 3C$, demonstrating the reversible utilization of CO_2.

Magnesium–CO_2 batteries have been recently explored, alongside aluminum and lithium CO_2 batteries, with limited primary research available on the subject. Mg is an appealing anode material due to its high reduction potential (-2.356 V), substantial specific capacity (2205 mAh/g), and abundant availability. Like Al–CO_2 batteries, the discharge product of magnesium bicarbonate is not well characterized. A primary cell utilizing a magnesium metal anode, nanostructured carbon cathode, and propylene carbonate electrolyte with magnesium perchlorate has been demonstrated (Fig. 6f) [126]. Furthermore, a novel aqueous, membrane-free rechargeable Mg–CO_2 battery employing KOH and NaCl salts has been recently introduced. This secondary Mg-CO_2 battery draws inspiration from aqueous Zn–CO_2 batteries but uniquely does not necessitate a pH differential between the anodic and cathodic electrolytes.

In a word, Li–CO_2 and Na–CO_2 batteries are considered as the most potential candidates for long-distance transportation due to their high operating voltages and large theoretical specific energy densities. They are especially suited for applications where CO_2 content is high, such as in submarines and space exploration. Meanwhile, K–CO_2 batteries utilize potassium ions because of their weak Lewis acidity and fast migration rate. Due to the high reactivity of alkali metal and limited range of carbonaceous products, Li–CO_2, Na–CO_2, and K–CO_2 batteries are typically operated in non-

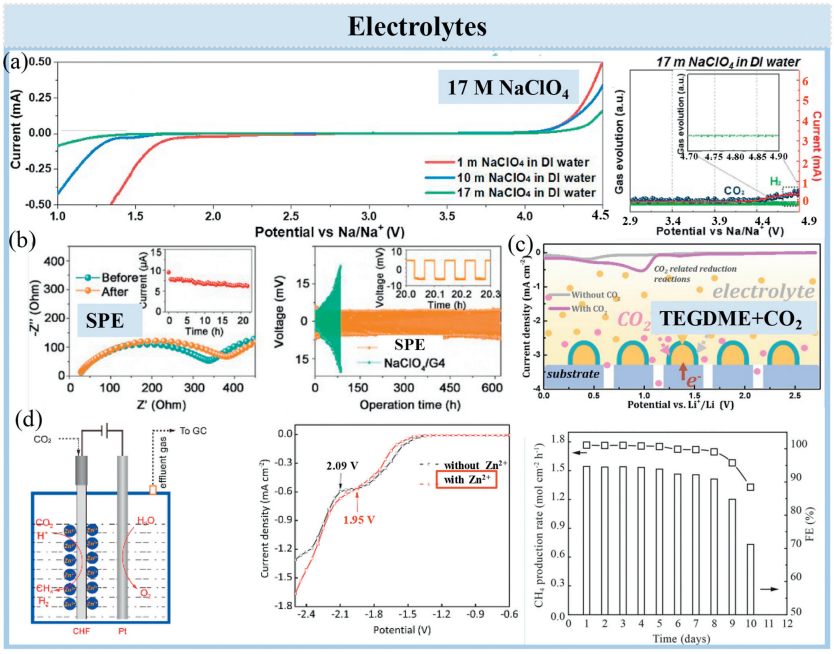


Fig. 7. (a) The performance of Na-CO_2 battery using 17 mol/L $NaClO_4$ electrolyte solution with a broad electrochemical window and the corresponding CO_2 evolution result. Copied with permission [128]. Copyright 2021, Elsevier. (b) Schematic illustration of SPE exhibiting good cycling stability and corresponding charge-discharge curve. Copied with permission [129]. Copyright 2021, Elsevier. (c) Schematic illustration of TEGDME and corresponding performance by introducing moderate CO_2 served as the gas additive with good stability. Copied with permission [127]. Copyright 2021, Elsevier. (d) Schematic illustration and the performances of regenerated Zn anode restored battery in a renewable Zn-CO_2 flow battery. Copied with permission [132]. Copyright 2021, Elsevier.

aqueous systems, which restricts their practical applications. Zn–CO_2 batteries are compatible with aqueous electrolytes, offering a lower operating voltage and energy density, and the highly selective production of carbonaceous chemicals such as CO and C_2H_4. Notably, Al–CO_2 batteries boast a higher specific energy compared to Zn and have the capability to upconvert captured CO_2 into oxalate, a precursor for various significant chemicals. Further research should be aimed at overcoming the main battery limitations, along with advancing CO_2 capture, and energy conversion and storage technologies.

4.2. Electrolytes

In metal-CO_2 batteries, the electrolyte plays a crucial role in facilitating the movement of ions between the cathode and anode during the charge and discharge processes. The electrolyte used in a metal-CO_2 battery needs to be able to dissolve CO_2 [109,127]. Drawing from the electrolytes used in Li-ion batteries can guide the choice for metal-CO_2 batteries. The currently reported electrolytes mainly include liquid electrolytes and solid-state electrolytes. The instability of the electrolyte system may be the greatest challenge faced by batteries. To achieve high-speed and stable transfer of metal ions in the electrolyte, three points related to the liquid solvents should be considered: (1) High dielectric constant and strong salt solubility to facilitate efficient metal ion transfer; (2) relatively low viscosity over a wide temperature range to minimize resistance to ion migration; (3) high electrochemical stability.

The economic aqueous electrolyte is particularly a good choice. Im *et al.* employed a 17 mol/L $NaClO_4$ electrolyte in Na-CO_2 batteries [128], effectively inhibiting H_2 evolution, broadening the electrochemical window, and providing a stable cycling performance without a significant electrolyte decomposition (Fig. 7a). However, the leakage resulting from the open battery structure, the electrochemical instability at high current density, and the volatilization in working conditions at high temperature, limited its practical application in metal-CO_2 batteries.

Simultaneously, all-solid-state polymer electrolyte (SPE) with the advantages of no liquid, good film-forming stability, flexibility, high mechanical strength is well applied to metal-CO_2 batteries [129,130]. Wang *et al.* designed integrated flexible Na-CO_2 batteries with SPE consisting of PEO/$NaClO_4$/3 wt% SiO_2 [129]. The application of SPE ensured the safety of the battery, which benefits from the use of solvent-free electrolyte and the uniform deposition of Na anode, exhibiting a good cycling stability (Fig. 7b). Qiu *et al.* improved the lithium bis(trifluoromethanesulfonyl)imide (LiTFSI)-TEGDME electrolyte by introducing moderate CO_2 served as the gas additive [127]. Sufficient CO_2 was helpful to form stable solid electrolyte interface (SEI) layers and protected the Li metal anode from rapid consumption, which efficiently improved the reversibility of the Li metal anode (Fig. 7c). These batteries usually convert CO_2 into solid-state products, such as amorphous carbon and oxalates, while Zn-CO_2 batteries can produce more value-added products [131]. Wang *et al.* assembled a renewable Zn-CO_2 flow battery, which could control the proton utilization rate by using a water-shuttling mechanism and selectively convert CO_2 into CH_4 within the hollow fiber [132]. In addition, the Zn anode was electrochemically renewed and the battery assembled with the regenerated Zn anode restored battery performances to the original level (Fig. 7d).

Although a solid-state electrolyte could suppress the ever-present issue of dendrite growth and is more stable than liquid electrolyte, the ionic conductivity of solid-state electrolytes is still low [133]. It is suggested that the future research associated with solid-state electrolyte should be focused more on raising the conductivity by following aspects: (1) Replacing of complexing salt anions by appropriate larger solvent ions, and (2) adding nanosized ceramic fillers to increase metal ions conductivity and improve the mechanical strength.

4.3. Anode interfacial interaction

Building a robust metal anode and choosing appropriate electrolyte are crucial steps in realizing stable metal-CO_2 batteries.

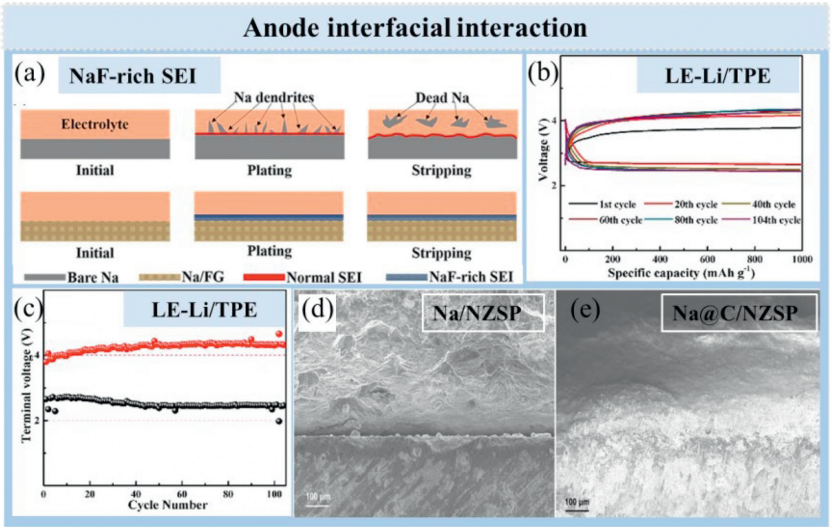


Fig. 8. (a) Schematic illustration of NaF-rich SEI layer function mechanism. Copied with permission [135]. Copyright 2021, Wiley. (b) Cycling life and (c) large discharge capacity of LE-Li/TPE. Copied with permission [136]. Copyright 2021, Elsevier. SEM images of good contact between anode and electrolyte of (d) Na/NZSP and (e) Na@C/NZSP. Copied with permission [137]. Copyright 2022, Elsevier.

Moreover, it is important to construct a stable interface between the metal anode and electrolyte. Unstable and poor contact between electrolyte and metal anode will result in large interfacial resistance and poor cycling stability. At the anode-electrolyte interface, the charge transfer resistance significantly impacts the charge-discharge efficiency and cycle stability of the battery. To mitigate interface impedance, material design should consider the following strategies: Surface modification of the electrode material, such as that incorporating conductive polymers or metal nanoparticles can enhance the active sites on the electrode surface and thereby improve the charge transfer kinetics. Additionally, constructing a protective layer on the electrode surface can effectively suppress the growth of lithium dendrites and decrease the charge transfer resistance at the interface.

Lu *et al.* reported an extremely simple approach to realize the compatible interface between the Na anode and electrolyte [134]. A compact NaF-rich interphase on a Na surface was introduced by a chemical reaction between fluoroethylene carbonate-Na^+ and Na metal, which not only prevented side reactions but also adjusted the uniform deposition of dendrite-free Na. Similarly, Mao *et al.* constructed a stable, NaF-rich SEI layer which could promote Na^+ conductivity, block electron transfer, suppress Na dendrite growth and inhibit reaction between Na anode and electrolyte (Fig. 8a) [135]. However, the traditional SEI layer formed by the reaction between Li anode and electrolyte is usually too fragile to stand on the dramatic electrode over cell operation.

Based on this, Chi *et al.* designed a stable artificial SEI layer by constructing the Li-ethylenediamine (LE) layer on Li anode and *in-situ* forming a tetraglyme-based polymer electrolyte (TPE) [136]. The uniform LE layer could effectively inhibit Li dendrites growth and obviously reduce the interface impedance between TPE and Li anode. Meanwhile, the synergy effect between LE layer and TPE apparently protected Li anode from CO_2 attacking. The LE-Li/TPE showed a superior cycling life, large discharge capacity, and low overpotential (Figs. 8b and c). Another strategy involves fabricating composite anodes to establish intimate contact. Tong *et al.* tackled the poor contact between Na metal anode and solid-state electrolyte $Na_3Zr_2Si_2PO_{12}$ (NZSP) by preparing a composite anode (Na@C) [137]. Mixing carbon black with melted Na metal formed the composite anode, which improved wetting of NZSP, decreased interfacial resistance, and extended cycling life (Figs. 8d and e).

In summary, the optimization of the protective layer is one of the key factors in enhancing the performance and safety of metal–CO_2 batteries. The optimization of the protective layer requires a comprehensive consideration of various factors, including the chemical stability, mechanical strength, electrical conductivity, and compatibility with the electrolyte and electrode materials of the protective layer. For instance, some studies have introduced nanostructured carbon materials as protective layers [137], which not only improve the electrical conductivity of the battery but also enhance the barrier ability of the protective layer to the electrolyte. Through surface treatment techniques, such as coating or plating, to enhance the adhesion between the protective layer and the metal anode [136], reducing interfacial resistance, thereby effectively improving the performance and safety of the battery.

However, there are several common challenges, such as dendrite growth and interphase problem between the anode and electrolyte. Dendrites, needle-like structures that form on the surface of the anode during cycling, pose a significant threat by potentially puncturing the separator and causing short circuits [113]. To mitigate dendrite growth, protective coatings or surface modifications on the anode have been explored [138,139]. For instance, Chen *et al.* reported that a carbon thin film deposited on Li metal anode (C/Li) by a sputtering system, which can effectively suppress the dendrite formation and prevent the underlying Li metal from the H_2O attack. The cell with the C/Li anode showed three times higher cyclability of 115 cycles at a high capacity of 500 mAh/g, as compared to that with pristine Li metal (Fig. 9a) [140]. The addition of rGO by Hu *et al.* [141] resulted in fast plating/stripping of nondendritic Na^+ on the rGO-Na anode and prevented the formation of Na dendrites even after 450 cycles at 500 mAh/g (Fig. 9b). However, the protective layer still eventually lost the metal protecting ability after the long-term electrochemical reaction. With the increase in the cycling numbers, the metal surface might progressively exposed and directly contacted the electrolyte, which finally caused the cell deterioration. Therefore, developing a robust protective layer for permanently conformally coating the metal anode can further enhance the cyclability of metal-CO_2 batteries in the future. This strategy provides a significant research direction focusing on the metal anode for elevating the metal-CO_2 battery durability.

In addition, the metal–CO_2 batteries loading excessive protective layer on the metal anode would generally lead to serious

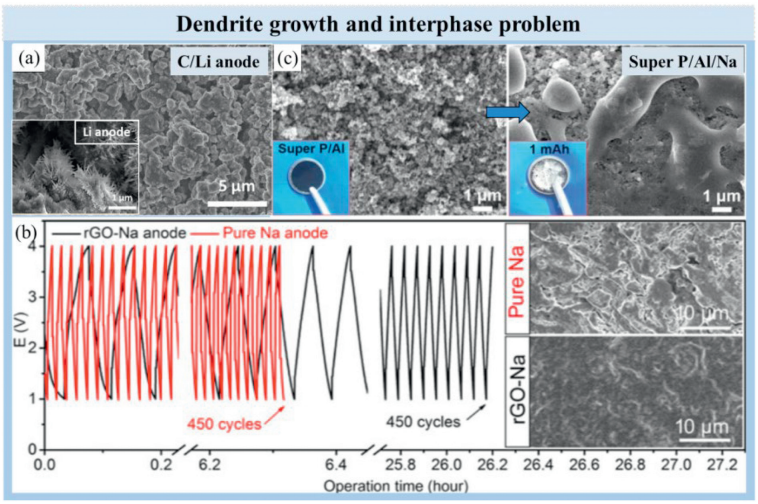


Fig. 9. SEM image of (a) C/Li anode in Li-CO_2 batteries after the cycling measurement. Copied with permission [140]. Copyright 2020, RSC. (b) The output potential of the Na-CO_2 batteries by using rGO-Na anode and pure Na anode and the corresponding SEM images. Copied with permission [141]. Copyright 2017, Science. (c) SEM images before and after performance test of Super P/Al/Na anode in Na-CO_2 batteries. Copied with permission [142]. Copyright 2018, AAAS.

safety problem and self-discharge. For this reason, Super P/Al, *i.e.*, Super P with diameter of 30 nm are coated on the surface of Al, which is used as anode by Sun *et al*. and dendrite-free Na could be quantitatively deposited on the anode because of its double advantage of possessing both large specific surface area and low nucleation barrier for Na plating, which can effectively reduce the formation of Na dendrite and improve the Coulombic efficiency of the battery (Fig. 9c) [142].

Overall, the decoration of a function layer on the metal or forming composite anode provides an avenue to suppress dendrite growth as well as stabilize the anode. In addition to the properties of the anode materials themselves, it can also be optimized by electrolyte to improve the performance of battery. SPE can not only satisfy the demand for flexible design, but also make up for the shortcomings of liquid electrolyte due to the merits of liquid-free, fine film-forming stability, flexibility, and mechanical strength. At the same time, the electrolyte should be stable relative to the anode and a stable interface phase should be formed between the anode and electrolyte, which can inhibit the dendrite growth and reduce the interface impedance. It is worth noting that metal-CO_2 batteries show high potential for carbon neutralization and electricity output. Ongoing research efforts should continue to focus on developing more effective strategies to improve the activity, stability, and efficiency of these batteries, ultimately advancing their practical applications in sustainable energy systems.

5. Summary and outlook

This review highlights various anode systems in eCO_2RR, offering novel insights for enhancing the stability and efficiency of CO_2 conversion. In electrocatalysis anode, IORs/OORs could replace the traditional OER, decreasing the cell voltage and producing more valuable chemicals. For metal-CO_2 battery anode, advancements in anode composite materials, suitable electrolytes, and stable interfaces are critical in mitigating dendrite growth and addressing interphase challenges. Photoanodes have seen significant improvements with advanced photoelectric materials, like Si photoanode, which could control electron-hole pair recombination and boost photo-to-electric conversion efficiency. Bio-anodes, involving microbial processes, utilize bacteria to oxidize waste organics, thereby increasing system current and lowering applied potential, leading to efficient chemical-to-electrical energy conversion. Notably, bio-anodes stand out due to their low cost, renewability, mild catalytic conditions, and the ability to produce a diverse range of valuable products from waste organics, aligning closely with the sustainable development goal of eCO_2RR (Fig. 10). Despite their promising features, bio-anodes still require substantial improvements and resolution for practical application challenges. Future research in this area can be carried out from the following aspects.

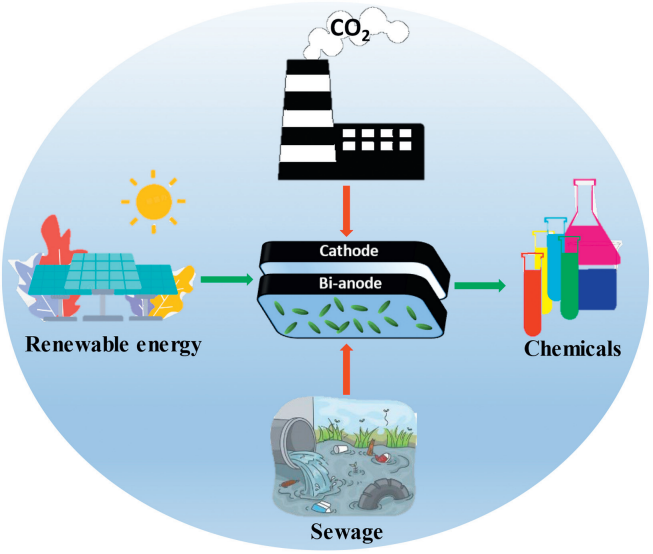


Fig. 10. Schematic illustration of an ideal bio-anode engineering mode for eCO_2RR to chemicals.

(1) Understanding the reaction mechanism of bio-anodes is crucial for advancing eCO_2RR technology. Currently, while density functional theory (DFT) calculations and real-time monitoring devices are extensively used to explore cathode mechanisms in eCO_2RR, anode reactions receive less attention. Integrating these mechanisms with experimental analysis is a key to designing CO_2 conversion reactor with enhanced stability, faster reaction rates, and superior CO_2 conversion efficiency. The ongoing research should also focus on improving the bacterial attachment with electrolyte and anode. Combining artificial nanomaterials with biofilms leads to higher bacterial cell densities and improved extracellular electron transfer efficiency.

(2) Minimizing carbon support corrosion is vital in electrochemical applications for eCO_2RR. Carbon is widely used in anodes as a gas diffusion layer and electrocatalyst support, thanks to its excellent electrical and thermal conductivity, mechanical properties, and high specific surface areas [143]. However, upon application of anode potential, carbon corrosion (carbon oxidation reaction, COR) occurs, leading to both soluble and insoluble organic and inorganic byproducts in the electrolyte, notably CO and CO_2. Ensuring long-term durability of anodic carbon is a significant challenge under industrialization current density, which should be paid more efforts [144–147].

Recent strategies have included the development of graphite carbon supports, such as acetylene black (AB) [148], multiwalled carbon nanotubes (MWCNTs) and carbon nanofibers [149,150]. These materials are more resistant to COR than disordered carbon supports, potentially improving anode and overall system performance [151]. Despite these advancements, carbon corrosion still results in irreversible catalyst loss. Lastly, alternatives to carbon substrates should also be explored. Ti-based anode, for example, is a promising substitute, although it can become passivated under anodic conditions, reducing electronic conductivity. Strategies to overcome this include shielding the Ti surface with a conductive film and modifying the passivation layer's conductivity through doping or surface engineering [152]. Although in bio-anode system, carbon corrosion is less frequently discussed, it remains important to develop specific strategies for these applications based on practical considerations.

In conclusion, coupling cathodic CO_2 reduction with cost-effective and efficient anodic reactions presents a viable and environmental-friendly method for transforming CO_2 into valuable chemicals, utilizing sustainable energy sources. Despite existing challenges in anode engineering, advancements in diverse anode technologies are progressively bringing these solutions closer to practical application. With ongoing, thorough research focused on anode development, CO_2 reduction technologies hold great promise for addressing greenhouse gas emissions and alleviating energy shortages.

Declaration of competing interest

The authors declare that they have no known competing financial interests or personal relationships that could have appeared to influence the work reported in this paper.

CRediT authorship contribution statement

Mingming Zhang: Writing – original draft. **Ting Xu:** Writing – review & editing, Validation. **Ruonan Yin:** Writing – original draft. **Xueqiu Chen:** Validation, Data curation. **Zheng-Jun Wang:** Validation, Supervision. **Jun Li:** Writing – review & editing, Data curation. **Xin Wang:** Validation, Supervision. **Huile Jin:** Validation, Supervision. **Haibo Ke:** Writing – review & editing, Validation, Supervision. **Shun Wang:** Writing – review & editing, Validation, Supervision. **Jing-Jing Lv:** Writing – review & editing, Validation, Supervision, Conceptualization.

Acknowledgments

This work was financially supported by the Open research fund of Songshan Lake Materials Laboratory (No. 2023SLABFN09), National Natural Science Foundation of China (Nos. 52201227, 52272088, 52331009), Chinese Education Ministry's Chunhui Program (No. 202200767), National Natural Science Foundation of China (No. 52401244), Zhejiang Provincial Natural Science Foundation of China (Nos. LQ23B030001, Q24B020025), and State Key Laboratory of Analytical Chemistry for Life Science (No. SKLACLS2411), China Postdoctoral Science Foundation (No. 2024M762442).

References

[1] H. Shin, K.U. Hansen, F. Jiao, Nat. Sustain. 4 (2021) 911–919.
[2] C. Kim, J.C. Bui, X. Luo, et al., Nat. Energy 6 (2021) 1026–1034.
[3] J.J. Lv, R. Yin, L. Zhou, et al., Angew. Chem. Int. Ed. 61 (2022) e202207252.
[4] D. Yang, B. Ni, X. Wang, Adv. Energy Mater. 10 (2020) 2001142.
[5] J.J. Lv, M. Jouny, W. Luc, et al., Adv. Mater. 30 (2018) 1803111.
[6] R.I. Masel, Z. Liu, H. Yang, et al., Nat. Nanotechnol. 16 (2021) 118–128.
[7] Z. Zhang, S. Li, Z. Zhang, et al., Carbon Energy 6 (2024) e513.
[8] M.C.O. Monteiro, M.F. Philips, K.J.P. Schouten, M.T.M. Koper, Nat. Commun. 12 (2021) 4943.
[9] B. Pan, J. Fan, J. Zhang, et al., ACS Energy Lett. 7 (2022) 4224–4231.
[10] H. Pan, C.J. Barile, Energy Environ. Sci. 13 (2020) 3567–3578.
[11] M. Jiang, H. Wang, M. Zhu, et al., Chem. Soc. Rev. 53 (2024) 5149–5189.
[12] D. Xu, K. Li, B. Jia, et al., Carbon Energy 5 (2023) e230.
[13] C. Xu, Y. Dong, H. Zhao, Y. Lei, Adv. Funct. 33 (2023) 2300926.
[14] C. Wang, Z. Lv, W. Yang, X. Feng, B. Wang, Chem. Soc. Rev. 52 (2023) 1382–1427.
[15] L. Liu, Y. He, Q. Li, et al., Exploration 4 (2024) 20230043.
[16] D.D. Ma, S.G. Han, S.H. Zhou, et al., CCS Chem. 5 (2022) 1827–1840.
[17] A. Vass, A. Kormanyos, Z. Koszo, B. Endrodi, C. Janaky, ACS Catal. 12 (2022) 1037–1051.
[18] S. Cheng, Z. Mao, Y. Sun, et al., Sci. Total Environ. 750 (2021) 141732.
[19] W. Xi, P. Yang, M. Jiang, et al., Appl. Catal. B: Environ. 341 (2024) 123291.
[20] W.A. Hika, A.R. Woldu, SN Appl. Sci. 3 (2021) 812.
[21] S. Verma, S. Lu, P.J.A. Kenis, Nat. Energy 4 (2019) 466–474.
[22] D. Li, J. Yang, J. Lian, J. Yan, S. Liu, J. Energy Chem. 77 (2023) 406–419.
[23] F. Ye, S. Zhang, Q. Cheng, et al., Nat. Commun. 14 (2023) 2040.
[24] Z. Xu, C. Peng, G. Zheng, Chem. Eur. J. 29 (2023) e202203147.
[25] S.Q. Liu, M.R. Gao, S. Wu, et al., Energ. Environ. Sci. 16 (2023) 5305–5314.
[26] P. Gupta, N. Verma, Chem. Eng. J. 446 (2022) 137029.
[27] F. Yang, Z. Ke, Z. Li, et al., ChemSusChem 13 (2020) 3391–3403.
[28] R.B. Song, W. Zhu, J. Fu, et al., Adv. Mater. 32 (2020) e1903796.
[29] F. Wang, Y. Li, X. Xia, et al., Adv. Energy Mater. 11 (2021) 2100667.
[30] J. Xie, Y. Wang, Acc. Chem. Res. 52 (2019) 1721–1729.
[31] Z. Li, S. Ning, J. Xu, et al., Energ. Environ. Sci. 15 (2022) 5300–5312.
[32] Q. Li, D.D. Ma, W.B. Wei, et al., Adv. Energy Mater. 14 (2024) 2401314.
[33] R. Ge, L.Y. Dong, X. Hu, et al., Chem. Eng. J. 438 (2022) 135500.
[34] V. Singh, T.C. Nagaiah, J. Mater. Chem. A 7 (2019) 10019–10029.
[35] M. Zhang, J. Guan, Y. Tu, et al., Energ. Environ. Sci. 13 (2020) 119–126.
[36] W. Ma, H. Wang, W. Yu, et al., Angew. Chem. Int. Ed. 57 (2018) 3473–3477.
[37] B. Zhang, J. Bai, Y. Zhang, et al., Environ. Sci. Technol. 55 (2021) 14854–14862.
[38] L. Yi, Y. Ji, P. Shao, et al., Angew. Chem. Int. Ed. 60 (2021) 21550–21557.
[39] M. Choi, J.W. Kim, S. Chung, et al., Chem. Eng. J. 430 (2022) 132563.
[40] C. Cao, D.D. Ma, J. Jia, et al., Adv. Mater. 33 (2021) 2008631.
[41] X. Wei, Y. Li, L. Chen, J. Shi, Angew. Chem. Int. Ed. 60 (2021) 3148–3155.
[42] M.A. Bajada, S. Roy, J. Warnan, et al., Angew. Chem. Int. Ed. 59 (2020) 15633–15641.
[43] X.V. Medvedeva, J.J. Medvedev, S.W. Tatarchuk, R.M. Choueiri, A. Klinkova, Green Chem. 22 (2020) 4456–4462.
[44] M. Gong, C. Cao, Q.L. Zhu, EnergyChem 5 (2023) 100111.
[45] J.H. Guo, W.Y. Sun, Appl. Catal. B: Environ. 275 (2020) 119154.
[46] C. Li, J. Shi, J. Liu, et al., Electrochim. Acta 389 (2021) 138728.
[47] X. Teng, K. Shi, L. Chen, J. Shi, Angew. Chem. Int. Ed. 63 (2024) e202318585.
[48] M. Qadir, P. Drechsel, B.Jiménez Cisneros, et al., Nat. Resour. Forum 44 (2020) 40–51.
[49] J. Na, B. Seo, J. Kim, et al., Nat. Commun. 10 (2019) 5193.
[50] Q. Zhang, Y. Chen, S. Yan, et al., Energ. Environ. Sci. 17 (2024) 2309–2314.
[51] M. Bevilacqua, J. Filippi, A. Lavacchi, et al., Energy Technol. 2 (2014) 522–525.
[52] E. Pérez-Gallent, S. Turk, R. Latsuzbaia, et al., Ind. Eng. Chem. Res. 58 (2019) 6195–6202.
[53] K. Xie, A. Ozden, R.K. Miao, et al., Nat. Commun. 13 (2022) 3070.
[54] G. Bharath, K. Rambabu, A. Hai, et al., Appl. Catal. B: Environ. 298 (2021) 120520.
[55] Y. Liang, W. Zhou, Y. Shi, C. Liu, B. Zhang, Sci. Bull. 65 (2020) 1547–1554.
[56] Y. Zhou, Z. Wang, W. Fang, et al., ACS Catal. 13 (2023) 2039–2046.
[57] Y. Li, C.Z. Huo, H.J. Wang, et al., Nano Energy 98 (2022) 107277.
[58] M.S.E. Houache, R. Safari, U.O. Nwabara, et al., ACS Appl. Energy Mater. 3 (2020) 8725–8738.
[59] T. Li, Y. Cao, J. He, C.P. Berlinguette, ACS Cent. Sci. 3 (2017) 778–783.
[60] Y. Wang, S. Gonell, U.R. Mathiyazhagan, et al., ACS Appl. Energy Mater. 2 (2018) 97–101.
[61] Y. Wang, X. Wei, Y. Li, et al., Chem. Eng. J. 485 (2024) 149800.
[62] M.A. Bajada, S. Roy, J. Warnan, et al., Angew. Chem. Int. Ed. 59 (2020) 15633–15641.
[63] Y. Li, C.Z. Huo, H.J. Wang, et al., Nano Energy 98 (2022) 107277.
[64] A. Kormányos, A. Szirmai, B. Endrődi, C. Janáky, ACS Catal. 14 (2024) 6503–6512.
[65] M.J. Llorente, B.H. Nguyen, C.P. Kubiak, K.D. Moeller, J. Am. Chem. Soc. 138 (2016) 15110–15113.

[66] S. Choi, M. Balamurugan, K.G. Lee, et al., J. Phys. Chem. Lett. 11 (2020) 2941–2948.
[67] Z.W. Yang, J.M. Chen, Z.L. Liang, et al., ChemCatChem 15 (2023) e202201321.
[68] G. Jia, Z. Wang, M. Gong, et al., Carbon Energy 5 (2022) e270.
[69] B. Liu, T. Wang, S. Wang, et al., Nat. Commun. 13 (2022) 7111.
[70] K. Wang, Y. Du, Y. Li, et al., Carbon Energy 5 (2022) e264.
[71] I. Merino-Garcia, S. Castro, A. Irabien, et al., J. Environ. Chem. Eng. 10 (2022) 107441.
[72] Y. Rambabu, U. Kumar, N. Singhal, et al., Appl. Surf. Sci. 485 (2019) 48–55.
[73] M. Li, Q. Wang, Y. He, et al., Coord. Chem. Rev. 495 (2023) 215373.
[74] W. Li, D. He, G. Hu, et al., ACS Cent. Sci. 4 (2018) 631–637.
[75] S. Castro, J. Albo, A. Irabien, J. Chem. Technol. Biotechnol. 95 (2020) 1876–1882.
[76] Y. Yu, F. Xie, R. Chen, et al., J. Power Sources 487 (2021) 229438.
[77] J. Zhang, S. Lv, J. Zheng, et al., ACS Sustainable Chem. Eng. 8 (2020) 11133–11140.
[78] D. Wang, Y. He, N. Zhong, et al., J. Hazard Mater. 410 (2021) 124563.
[79] W.A. Thompson, C. Perier, M.M. Maroto-Valer, Appl. Catal. B: Environ. 238 (2018) 136–146.
[80] Y.P. Peng, Y.T. Yeh, S.I. Shah, C.P. Huang, Appl. Catal. B: Environ. 123-124 (2012) 414–423.
[81] M. Zhang, J. Cheng, X. Xuan, J. Zhou, K. Cen, ACS Sustain. Chem. Eng. 4 (2016) 6344–6354.
[82] J.F.d. Brito, J.A.L. Perini, S. Perathoner, M.V.B. Zanoni, Electrochim. Acta 306 (2019) 277–284.
[83] R.A.N. Khasanah, H.C. Lin, H.Y. Ho, et al., RSC Adv. 11 (2021) 4935–4941.
[84] Y. Liu, L. Deng, J. Sheng, et al., Appl. Surf. Sci. 498 (2019) 143899.
[85] Z. Xu, S. Zhang, F. Gao, et al., Electrochim. Acta 324 (2019) 134844.
[86] G. Chen, H. Li, H. Zhang, et al., Res. Chem. Intermed. 47 (2021) 4825–4835.
[87] Z. Xing, X. Zhang, W. Yang, et al., Nanotechnology 32 (2021) 505705.
[88] M. Higashi, I. Tanaka, Y. Amao, T. Yoshida, New J. Chem. 46 (2022) 5932–5938.
[89] Z. Lian, D. Pan, W. Wang, et al., J. Environ. Sci. 60 (2017) 108–113.
[90] Gurudayal, J.W. Beeman, J. Bullock, et al., Energ. Environ. Sci. 12 (2019) 1068–1077.
[91] F. Sahli, J. Werner, B.A. Kamino, et al., Nat. Mater. 17 (2018) 820–826.
[92] G. Kanellos, E. Monokrousou, A. Tremouli, G. Lyberatos, Sustain. Chem. Pharm. 39 (2024) 101589.
[93] L. Lu, Z. Li, X. Chen, et al., Joule 4 (2020) 2149–2161.
[94] V. Sivalingam, C. Dinamarca, G. Samarakoon, D. Winkler, R. Bakke, Sustainability 12 (2020) 3081.
[95] Y. Tian, D. Li, G. Liu, et al., Bioresour Technol 320 (2021) 124292.
[96] R.A. Bullen, T.C. Arnot, J.B. Lakeman, F.C. Walsh, Biosens. Bioelectron. 21 (2006) 2015–2045.
[97] H. Guo, J. Hua, J. Cheng, L. Yue, J. Zhou, J. Cleaner Prod. 358 (2022) 131983.
[98] Y.X. Huang, Z. Hu, Fuel 220 (2018) 8–13.
[99] M. Zeppilli, D. Pavesi, M. Gottardo, et al., Chem. Eng. J. 328 (2017) 428–433.
[100] T. Luo, Q. Song, J. Han, Y. Li, L. Liu, Sep. Purif. Technol. 280 (2022) 119437.
[101] Z. Zhao, Y. zhang, Y. Li, H. Zhao, X. Quan, Water Res. 106 (2016) 339–343.
[102] A. Kokkoli, Y. Zhang, I. Angelidaki, Bioresour Technol. 247 (2018) 380–386.
[103] L. Cristiani, J. Ferretti, M. Zeppilli, Chem. Eng. Technol. 45 (2021) 365–371.
[104] C.M. Dykstra, S.G. Pavlostathis, Water Res. 200 (2021) 117268.
[105] T. Zheng, M. Zhang, L. Wu, et al., Nat. Catal. 5 (2022) 388–396.
[106] T. Haas, R. Krause, R. Weber, M. Demler, G. Schmid, Nat. Catal. 1 (2018) 32–39.
[107] C.J. Fetrow, C. Carugati, X.D. Zhou, S. Wei, Energy Storage Mater. 45 (2022) 911–933.
[108] W. Ma, X. Liu, C. Li, et al., Adv. Mater. 30 (2018) e1801152.
[109] X. Mu, H. Pan, P. He, H. Zhou, Adv. Mater. 32 (2020) e1903790.
[110] X. Wang, J. Xie, M.A. Ghausi, et al., Adv. Mater. 31 (2019) e1807807.
[111] J. Lu, S. Zhang, J. Yao, et al., ACS Nano 18 (2024) 10930–10945.
[112] J. Gabski, X. Sun, L. Iskhakova, J. Dong, J. Mater. Chem. A 12 (2024) 4441–4446.
[113] C. Xu, K. Zhang, D. Zhang, et al., Nano Energy 68 (2020) 104318.
[114] Z. Zhang, W.L. Bai, K.X. Wang, J.S. Chen, Energ. Environ. Sci. 13 (2020) 4717–4737.
[115] Y. Liu, R. Wang, Y. Lyu, H. Li, L. Chen, Energ. Environ. Sci. 7 (2014) 677–681.
[116] J. Lin, J. Ding, H. Wang, et al., Adv. Mater. 34 (2022) 2200559.
[117] Y. Xiao, S. Hu, Y. Miao, et al., Small 20 (2024) 2305009.
[118] J. Zou, G. Liang, J.A. Yuwono, et al., ACS Energy Lett. 9 (2024) 5145–5155.
[119] X. Hu, J. Sun, Z. Li, et al., Angew. Chem. Int. Ed. 55 (2016) 6482–6486.
[120] W. Zhang, C. Hu, Z. Guo, L. Dai, Angew. Chem. Int. Ed. 59 (2020) 3470–3474.
[121] W. Ma, X. Liu, C. Li, et al., Adv. Mater. 30 (2018) 1801152.
[122] J. Xie, Y. Wang, Acc. Chem. Res. 52 (2019) 1721–1729.
[123] J. Xie, X. Wang, J. Lv, et al., Angew. Chem. Int. Ed. 57 (2018) 16996–17001.
[124] C. Fetrow, C. Carugati, X. Yu, X.D. Zhou, S. Wei, ACS Appl. Mater. Inter. 15 (2023) 12908–12914.
[125] Y. Luo, S. Chen, J. Zhang, et al., Adv. Mater. 35 (2023) 2303297.
[126] J. Kim, A. Seong, Y. Yang, et al., Nano Energy 82 (2021) 105741.
[127] F. Qiu, S. Ren, X. Mu, et al., Energy Storage Mater. 26 (2020) 443–447.
[128] E. Im, J.H. Ryu, K. Baek, G.D. Moon, S.J. Kang, Energy Storage Mater. 37 (2021) 424–432.
[129] X. Wang, X. Zhang, Y. Lu, et al., ChemElectroChem 5 (2018) 3628–3632.
[130] X. Hu, Z. Li, Y. Zhao, et al., J. Chen, Sci. Adv. 3 (2017) e1602396.
[131] Z. Zheng, C. Wang, P. Mao, et al., Carbon Energy 5 (2022) e274.
[132] K. Wang, Y. Wu, X. Cao, L. Gu, J. Hu, Adv. Funct. 30 (2020) 1908965.
[133] R.C. Agrawal, G.P. Pandey, J. Phys. D: Appl. Phys. 41 (2008) 223001.
[134] Y. Lu, Y. Cai, Q. Zhang, et al., Chem. Sci. 10 (2019) 4306–4312.
[135] Y. Mao, X. Chen, H. Cheng, et al., Energy Environ. Mater. 5 (2021) 572–581.
[136] S. Zhang, X. Liu, Y. Feng, et al., J. Power Sources 506 (2021) 230226.
[137] Z. Tong, S.B. Wang, Y.C. Wang, et al., J. Alloys Compd. 922 (2022) 166123.
[138] Z. Liang, G. Zheng, C. Liu, et al., Nano Lett. 15 (2015) 2910–2916.
[139] K. Liu, A. Pei, H.R. Lee, et al., J Am. Chem. Soc. 139 (2017) 4815–4820.
[140] C.J. Chen, J.J. Yang, C.H. Chen, et al., Nanoscale 12 (2020) 8385–8396.
[141] X. Hu, Z. Li, Y. Zhao, et al., Chen, Sci. Adv. 3 (2017) e1602396.
[142] J. Sun, Y. Lu, H. Yang, et al., Research 2018 (2018) 6914626.
[143] T. Xu, H. Huang, T. Lu, et al., Carbon 205 (2023) 207–213.
[144] D. Liu, K. Ni, J. Ye, et al., Adv. Mater. 30 (2018) 1802104.
[145] Y. Wang, P. Yang, L. Zheng, X. Shi, H. Zheng, Energy Stor. Mater. 26 (2020) 349–370.
[146] Y. Xiang, L. Lu, A.G.P. Kottapalli, Y. Pei, Carbon Energy 4 (2022) 346–398.
[147] M. Zhong, M. Zhang, X. Li, Carbon Energy 4 (2022) 950–985.
[148] J.A. Prithi, R. Vedarajan, G.Ranga Rao, N. Rajalakshmi, Int. J. Hydrogen Energy 46 (2021) 17871–17885.
[149] S.W. Lee, S.R. Choi, J. Jang, et al., J. Mater. Chem. A 7 (2019) 25056–25065.
[150] D. Jia, X. Yu, T. Chen, et al., J. Power Sources 358 (2017) 13–21.
[151] L. Castanheira, W.O. Silva, F.H.B. Lima, et al., ACS Catal. 5 (2015) 2184–2194.
[152] H. Jang, S. Chung, J. Lee, Electrochim. Acta 365 (2021) 137276.